A fundamental study of corrosion-resistant zinc-nickel electroplating

By

Dr. Kei Higashi, project leader, and Dr. Yasunori Hayashi,
Dr. Hisaaki Fukushima, Dr. Tetsuya Akiyama and Dr. Hideki Hagi

CONTENTS

1. Introduction.

The mechanical and chemical properties of metals are considerably improved by alloying. In recent years, the electrodeposition of alloys has aroused an intense interest as a new technique which has great industrial possibilities for producing coatings of higher quality in the field of surface finishing as well as for the hydrometallurgical production of new materials such as intermetallic compounds, supersaturated solid solutions and amorphous alloys which cannot be obtained pyrometallurgically.

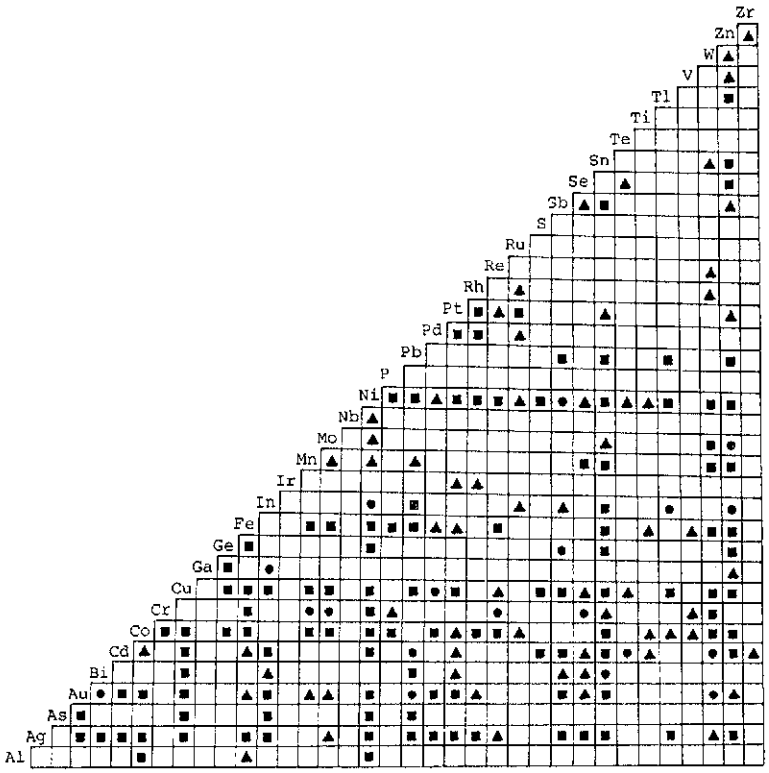

Fig.l Binary alloys which have been electrodeposited from aqueous solution: ■ indicates alloys reported up to 1960, • indicates alloys electrodeposited for the first time between 1961 and 1964, and ▲ indicates alloys reported since 1964.

Electrode position of alloys has a 147 year long history which goes back to brass plating by Jacobi in 1841, and so far attempts have been made to electrodeposit more than 200 kinds of binary and ternary alloys from aqueous solutions as shown in Fig.l [1]. Approximately 70 kinds of alloys, more than one third of those reported previously, contain iron-group metal. The number of alloy systems amounts to 30 for Ni alloys, 23 for Co alloys and 21 for Fe alloys. Thus, of the iron-group metals, Ni appeared most frequently as a constituent in all alloy systems. A survey of the large amount of literature published between 1975 and 1984 has revealed that about 80 % of this literature is concerned with alloy systems containing iron-group metal,

especially Ni, as shown in Table 1. Among the Ni alloys, Ni-Zn, Ni-Fe and Ni-Sn are the systems investigated most actively because the deposit obtained has been expected to possess an outstanding favorable property for practical use and further because their electrodeposition behavior is interesting from an academic point of view. Figure 2 shows chronologically the number of reports on the above three systems in the last 12 years. In each year, an intense study has been conducted of the electrodeposition of Ni-Fe and Ni-Sn systems for decorative, corrosion-resistant or magnetic alloy plating. On the other hand, the number of reports on Ni-Zn alloys began to increase abruptly from the beginning of the 1980's. This trend has mainly resulted from the frantic research by steel manufacturers to develop highly corrosion-resistant alloy plated steel sheet for automotive body panels [2]-[6].

In order to promote the practical use of this highly corrosion-resistant Ni-Zn alloy in other fields of metal finishing as well as in the automotive industry, a comprehensive knowledge of Ni-Zn alloy plating is required.

The authors have been granted financial support by the Nickel Development Institute to conduct a series of studies on Zn-Ni alloy plating. This is the final report submitted to the Institute.

Table 1 Percentage of metals used as an alloying element. A survey from recent reports on alloy deposition (1975-1984).

	'75	'76	'77	'78	'79	'80	'81	'82	'83	'84
Ni	40.0	41.0	46.3	38.0	41.9	26.5	39.1	40.0	55.5	48.7
Co	23.0	19.7	20.7	35.4	30.1	18.4	16.3	16.7	10.6	15.7
Fe	19.7	13.1	18.3	6.3	14.0	7.1	21.7	22.2	17.6	19.1
Zn	3.3	18.0	14.6	11.4	7.5	17.3	18.5	24.4	47.1	35.7
Sn	24.6	27.9	12.2	20.3	17.2	20.4	13.0	24.4	12.9	13.9
Cu	16.4	17.7	12.2	20.3	18.3	14.3	13.0	7.8	8.2	13.0
Au	13.1	18.0	12.2	10.1	18.3	14.3	14.1	14.4	5.9	8.7
Pb	11.5	9.8	9.8	8.9	5.4	16.3	10.9	13.3	8.2	6.1
Cr	4.9	6.6	11.0	5.1	9.7	4.1	10.9	6.7	5.9	7.0
Cd	3.3	14.8	9.8	6.3	6.5	7.1	6.5	5.6	3.5	7.8
*	61	61	82	79	93	98	92	90	85	115

* Total number of reports.

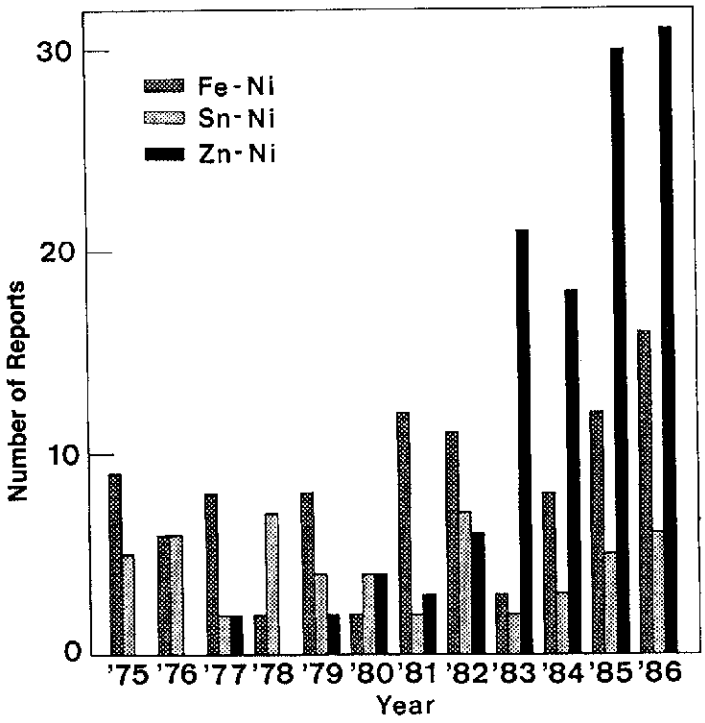

Fig.2 Annual number of reports on the electrodeposition of Fe-Ni, Sn-Ni and Zn-Ni alloys.

2. Fundamental electrodeposition process for Zn-Ni alloys.

2-1 General feature of anomalous alloy deposition.

In the simultaneous discharge of different metal ions whose equilibrium potentials do not differ too much from each other, the more noble metal is generally deposited preferentially because of the greater driving force for its deposition. When the single electrode potentials of the metals differ too much, their equilibrium potentials are difficult to bring close together by alteration of the metal ion concentration ratio in a solution, and the cathode is hardly polarized to the equilibrium potential of the less noble metal. Therefore, alloys cannot be deposited unless the activity of the more noble metal ion in a solution is greatly decreased by a stable complex formation. On the other hand, in the electrodeposition of iron-group metal alloys with Zn or Cd, as well as the mutual alloys of iron-group metals such as Fe-Ni and Fe-Co, such an anomaly appears as the preferential deposition of the less noble metal even in the simultaneous discharge of hydrated ions. These alloy depositions are called 'anomalous type' [7].

In all alloy systems presented above, the iron-group metal is necessarily more noble than the other constituent, and anomalous alloy deposition never occurs in an alloy system such as Cu-iron-group metal, where the iron-group metal is the less noble constituent. The metals which are less noble than iron-group metals (standard electrode potentials are -0.25, -0.28 and -0.44 V vs. NHE for Ni, Co and Fe, respectively [8]) and are capable of being deposited from hydrated ions on a solid electrode at significant current efficiency are limited to a small number of metals: Cd (-0.40 V); Zn (-0.76 V); and Mn (-1.18 V) [9]. This leads to the fact that anomalous deposition occurs only in the relatively small number of alloys described above.

2-2 Properties peculiar to iron-group metals which may be related to the appearance of anomaly in the electrodeposition of alloys.

Besides the anomalous type, there is an another type of abnormal alloy deposition called 'induced type' where a reluctant metal such as Mo or W, which cannot be deposited alone, deposits with an inducing iron-group metal [7]. It is very interesting that an iron-group metal is necessarily one of the constituents of alloy systems where anomaly appears. This implies that the appearance of anomaly in alloy deposition should be attributed to the properties peculiar to iron-group metals.

Since the electrodeposition of metals from aqueous solutions is intimately associated with a competitive hydrogen evolution reaction, the deposition capability of a certain metal should be determined by the relative discharge rates of both hydrogen and metal ions on this metal. This means that the properties of the metal in both metallic and ionic states determine the deposition capability of the metal, because the standard potential of a metal/metal ion electrode depends on the stability, and hence the properties, of the metallic element in both states, while hydrogen overpotential depends on the properties in the metallic state.

Properties in the ionic state:

Among metals which can be deposited from aqueous solutions by themselves, only iron-group metals possess deposition overpotential, i.e., iron-group metals begin to deposit at potentials which are several tenths of a volt less noble than their equilibrium values [10], while most other metals begin to deposit at their equilibrium potentials. This means that the deposition sites for iron-group metals are substantially limited on the cathode. Therefore, the deposition of iron-group metals is easily further polarized when their deposition sites are occupied by adsorbed foreign substances. On the other hand, since the deposition of iron-group metals is depressed apparently but not thermodynamically at the potentials less noble than their equilibrium potentials, their deposition can be depolarized toward their equilibrium potentials in the presence of certain catalysts. It is well known in the polarographic study of Ni deposition that the catalytic pre-wave due to anion bridging, or surface chelation, is observed when S- and N-compounds are present in the electrolyte [11]-[16]. Thus, the deposition potentials, and hence the apparent equilibrium potentials, of iron-group metals tend to be affected remarkably by the adsorption of such foreign substances as inhibitor or catalyst on the sites.

It is well known that hydrogen, as well as iron-group metals, has a deposition overpotential which is generally called hydrogen overpotential. Hydrogen evolution on Hg which has high hydrogen overpotential is considerably depolarized in the presence of S- and N-compounds [17]. This indicates that hydrogen possesses the same property as iron-group metals. Since the behavior of hydrogen ion must always be considered in a metal deposition from aqueous solutions, constant attention should be paid to this property.

Properties in the metallic state:

Of the metals which can be deposited from aqueous solutions by themselves, only iron-group metals are ferromagnetic. This is caused by the electronic structure of iron-group metals, which differs from other metals to such a degree that they have decimal numbers of unpaired electrons (Fe 2.2, Co 1.6, Ni 0.6), due to the unequal distribution of the holes in two 3d sub-bands [18]. The existence of these unpaired electrons provides iron-group metals with the highest heat of adsorption of atomic hydrogen among the metals which can be

Table 2 Heats of adsorption of atomic hydrogen on various metals (kJ/mol).

Ag*	Al	Au*	Be	Cd*	Cr	Cu*	Fe*	Ga*
240.6	242.7	248.2	243.6	225.6	251.5	244.8	253.2	236.5
Hg*	In*	Mg	Mn	Mo	Nb	Ni*	Pb*	Pd
221.4	236.5	228.9	240.6	275.4	283.3	251.9	232.7	249.0
Pt	Ta	Ti	Tl*	V	W	Zn*		
263.2	287.1	255.3	231.4	258.2	287.1	229.8		

* Metal which can be electrodeposited from aqueous solution with high current efficiency.

deposited from aqueous solutions with high cathode current efficiency (Table 2) [19], as well as a high affinity for adsorbing S- and N-compounds which have lone pairs of electrons [20]. Thus, iron-group metals possess a high ability of holding such substances as atomic hydrogen and S-, N-compounds on their surface.

On the basis of the properties peculiar to iron-group metals described above, the present authors have already proposed a possible mechanism for the induced codeposition of Mo with iron-group metals and explained that the induced type alloy deposition proceeded under conditions where the favorable aspects of the properties of iron-group metals, i.e., the depolarization of iron-group metal deposition and the high ability to hold atomic hydrogen, were allowed to function in good combination, whereas alloy deposition never occurred under conditions where the properties in the metallic state were not able to function satisfactorily due to the unfavorable properties in the ionic state, i.e., the polarization of iron-group metal deposition [21]-[27].

In anomalous alloy deposition where alloys of low iron-group metal content are normally obtained, on the other hand, the properties of iron-group metals in the metallic state may play no role because the 3d bands of iron-group metals are filled up with 4s electrons from Zn in alloys of Zn with iron-group metals, for example.

2-3 Hydroxide suppression mechanism.

In the sulfate baths, both iron-group metal and Zn exist in their simplest form of hydrated ion. Ni begins to deposit from a sulfate bath containing, for example, 0.9 mol/1 of metal ion at about -0.43 V vs. NHE which is 0.18 V less noble than its equilibrium potential, -0.25 V [28]. Ni, as well as other iron-group metals, thus has an inherent deposition overpotential. However, this deposition overpotential is not large enough to bring the apparent equilibrium potential of Ni at which Ni begins to deposit to the equilibrium potential of Zn, -0.76 V when Zn ion concentration is 1 mol/l. Thus, it is impossible to explain the preferential deposition of Zn, which is considerably less noble than iron-group metals, by considering only the inherent large deposition overpotential of the iron-group metals. As mentioned previously, the electrodeposition of iron-group metal tends to be easily affected by the adsorption of such foreign substances as inhibitor or catalyst on their deposition sites. In order to make the preferential deposition of Zn possible, therefore, the presence of an inhibitor for iron-group metal deposition must be necessary. In the electrodeposition of Zn-iron-group metal alloys, the metal hydroxide formed by hydrolysis due to the pH rise in the vicinity of cathode has been regarded as such an inhibitor [29],[30].

2-3-1 Transition of alloy deposition behavior from a normal to an anomalous type and the formation of Zn hydroxide [31],[32].

In anomalous alloy deposition, generally, the change in alloy composition produced by alteration of plating variables hardly exhibits a definite tendency [7], and this is observed most

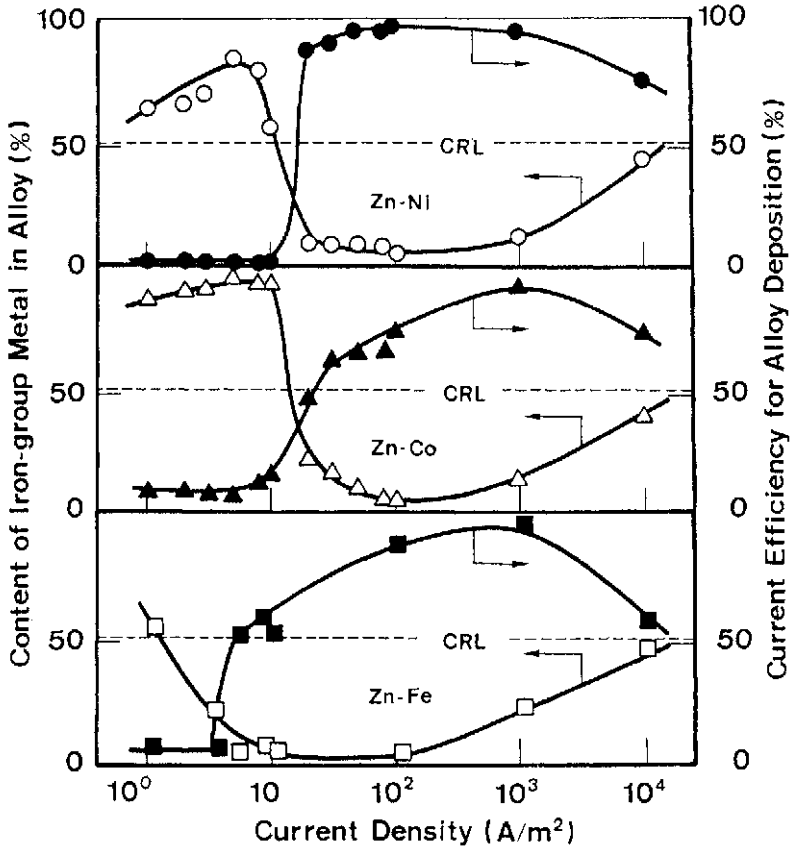

Fig. 3 Effect of current density on the electrodeposited alloy composition and on the cathode current efficiency for alloy deposition.

characteristically when the current density is varied. Figure 3 gives experimental results showing the effect of current density on the alloy composition and current efficiency for alloy deposition. The standard plating conditions are shown in Table 3. The segmented line in Fig.3 indicates the composition reference line (hereinafter simply referred to as CRL) which shows when the weight-percentage composition of the alloy just equals the metal-percentage in the bath. In the case

Table 3 Standard plating conditions for Zn-iron-group metal alloys.

Bath composition		Operating condition	
Zinc sulfate	0.5 mol/l	Current density	10 A/dm^2
Iron-group metal sulfate	0.5 mol/l	Temperature	40 °C
Sodium acetate	0.2 mol/1	Electrolysis duration	100 s
Sulfuric acid	*	Quiescent bath	

* Necessary amount for adjusting pH of the solution to 3.0

in which iron-group metal content of the alloy lies above the CRL, electrodeposition of normal type occurs, because the alloys contain a larger ratio of iron-group metal to Zn than the bath, and hence the electrochemically more noble iron-group metal deposits preferentially. On the other hand, iron-group metal contents below the CRL represent anomalous codeposition in which the preferential deposition of less noble Zn occurs.

At low current densities, the codeposition was of the normal type while the cathode current efficiency was extremely poor, indicating predominant hydrogen evolution. With increasing current density, the content of iron-group metal in the alloys rapidly decreased and the current efficiency increased correspondingly. The current density at which the electrodeposition behavior of the alloys thus changes from a normal to an anomalous type is called the transition current density [7]. Further increase in the current density resulted in little change in alloy composition, followed by the trend that iron-group metal content increased gradually upward to attain the CRL at still higher current densities. The alloy deposition behavior at higher current densities than the transition current density is discussed later in detail in connection with the anomalous codeposition of Ni with Zn.

The alloys were next electrodeposited under the same conditions as in the deposition study shown in Fig.3, and pH in the cathode layer (at the position exactly 10 μm from the cathode) was simultaneously measured by means of the Sb microelectrode technique[33]. Results are summarized in Fig.4 in which the relationship between the alloy composition and the pH in the vicinity of the cathode is presented. The figure also includes the CRL, the pH of a bulk solution and the

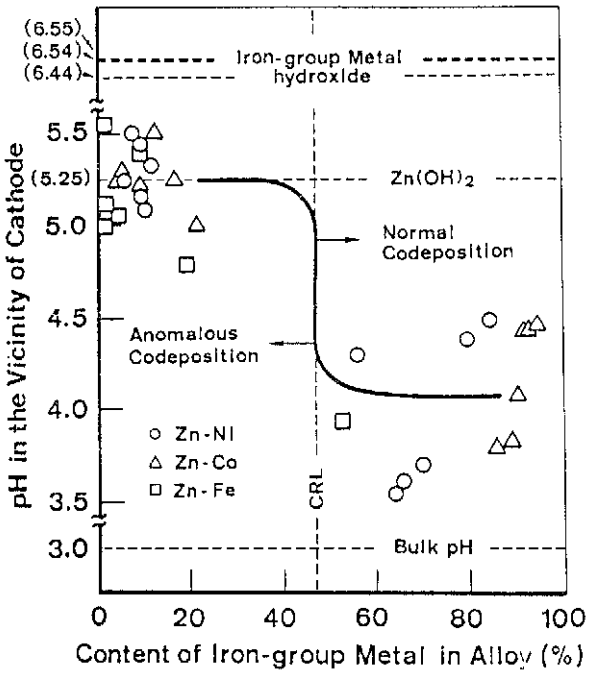

Fig.4 Relationship between the composition of alloys and pH in the vicinity of the cathode during the electrode position of Zn-iron-group metal alloys.

critical pH values for each metal hydroxide precipitation determined by measuring their solubilities at various pH's in the bath used. Figure 4 showed that the critical pH for Zn hydroxide precipitation was not attained in the normal codeposition region although a rise in pH of the cathode layer, when compared with the bulk solution, was observed to some extent. On the other hand, an abrupt rise in the pH took place, permitting Zn hydroxide precipitation, when the transition of codeposition from a normal to an anomalous type occurred. In the anomalous codeposition region, the pH of the cathode layer remained at a value around the critical pH for Zn hydroxide precipitation which was well below the critical one for iron-group metal hydroxides.

2-3-2 Mechanism of the abrupt transition from a normal to an anomalous type alloy deposition at the transition current density.

In the sulfate bath used, the ions which are capable of being discharged at the cathode are those of hydrogen, iron-group metal and Zn, and exist in the simplest form of hydrated ions. Of these ions, as mentioned previously, Zn, like most other metals, begins to deposit at its equilibrium potential while iron-group metal and hydrogen have the inherent property of not beginning to deposit at their equilibrium potentials but requiring an extra overpotential.

As presented in 2-3-1, the normal-type alloy deposition occurs with extremely poor current efficiency at lower current densities before the transition, whereas the anomalous type alloy deposition proceeds with relatively high current efficiency after the transition current density is achieved.

In the low current density region, each depositable ion exists in an ionic form in the cathode layer because the critical pH for the precipitation of Zn hydroxide as well as the one for iron-group metal hydroxide is not attained (Fig.4). Since the apparent equilibrium potentials of hydrogen and iron-group metals are not polarized to exceed the equilibrium potential of Zn even though their depositions are inherently polarized, the respective nobilities of depositable hydrogen and metals should be directly reflected in their depositing behaviors during simultaneous deposition. Therefore, the most noble hydrogen discharges preferentially and then iron-group metal deposits slightly, which causes the poor current efficiency for the alloy deposition of normal type.

As the current density is raised, pH in the cathode layer rises due to the increased rate of hydrogen evolution, which results in Zn hydroxide formation and subsequent adsorption on the cathode, while iron-group metals in the cathode layer exist in an ionic form because the solution is buffered by Zn hydrolysis at a pH well below the critical pH for the precipitation of these metal hydroxides. Then, the apparent equilibrium potentials of iron-group metal and hydrogen, whose deposition potentials inherently tend to be affected by the adsorption of foreign substances, are further polarized and the driving force for their deposition is substantially decreased. When the electrolysis is conducted under galvanostatic conditions, this leads to the abrupt polarization of the cathode at the transition current density toward the deposition potential of the next depositable ion, Zn. Since the equilibrium potentials for Zn deposition from the hydrated ion and from its hydroxide are thermodynamically identical at the critical pH for Zn hydroxide

precipitation, it is not necessary to consider the change in the equilibrium potential due to the formation of Zn hydroxide. Therefore, Zn deposition begins and proceeds easily with preceding hydroxide formation when the cathode is polarized to reach its deposition potential. Since the apparent equilibrium potential of iron-group metal is considered to be polarized to exceed that of Zn, and hydrogen evolution is further depressed by the large hydrogen overpotential on Zn together with the polarization due to the adsorbed Zn hydroxide, the anomalous alloy deposition proceeds with high current efficiency.

At present, the above explanation proposed by the authors is considered to be most plausible and is called the hydroxide suppression mechanism [30].

2-3-3 Effect of the buffer capacity of a Zn-Ni alloy plating bath on the transition current density – Confirmation of the hydroxide suppression mechanism [34].

According to the hydroxide suppression mechanism, the transition current density is approximately identical to the required minimum current density of hydrogen discharge which brings the pH of the cathode layer to the critical value for Zn hydroxide precipitation, because hydrogen evolution is predominant in the low current density region where the normal-type alloy deposition occurs. Therefore, any change in plating conditions which prevents a rise in pH in the cathode layer will make the transition from a normal to an anomalous type alloy deposition difficult by increasing the transition current density.

Therefore, alloys were electrodeposited at various current densities from several baths listed in Table 4 and the transition current density in each bath was determined. The transition current densities were plotted in Fig.5 as a function of the buffer capacity expressed as the theoretical amount of sodium hydroxide required to bring about Zn hydroxide precipitation in each bath. As shown in Fig.5, the transition current density increased in proportion to the increase in the buffer capacity of the bath, indicating the validity of the hydroxide suppression mechanism.

It is reported that the transition current density is lower when conditions favor high metal depletion in the cathode diffusion layer, e.g., at low temperature or in baths having a low total metal ion concentration [7],[30]. As shown in Fig.5, however, the transitions were observed at almost the same current density of 0.1 A/dm^2 for

Table 4 Composition and buffer capacity of bath.

Bath No.	1	2	3	4	5	6	7	8	9	10	11	12	13	14	15	16
$ZnSO_4 \bullet 7H_2O$	0.5	0.5	0.5	0.5	0.5	0.5	0.5	0.5	0.5	0.5	0.5	0.5	0.3	0.1	0.1	0.05
$NiSO_4 \bullet 6H_20$	0.5	0.5	0.5	0.5	0.5	0.5	0.5	0.5	0.5	0.5	0.5	0,5	0.7	0.9	0.1	0.05
Na_2SO_4	-	-	-	-	-	0.5	0.5	-	-	-	-	-	-	-	0.8	0.9
$CH_3COONa \bullet 3H_2O$	-	-	-	-	-	-	-	0.5	0.05	0.2	0.5	1.0	0.2	0.2	0.2	0.2
H_2SO_4	*	*	*	*	*	*	*	*	*	*	*	*	*	*	*	*
pH	1.0	1.5	2.0	2.5	3.0	1.0	2.0	2.0	3.0	3.0	3.0	3.0	3.0	3.0	3.0	3.0
Metal- % of Ni in bath	47.3	47.3	47.3	47.3	47.3	47.3	47.3	47.3	47.3	47.3	47.3	47.3	67.7	89.0	47.3	47.3
Total metal ion conc.	1.0	1.0	1.0	1.0	1.0	1.0	1.0	1.0	1.0	1.0	1.0	1.0	1.0	1.0	0.2	0.1
Buffer capacity	1.84	1.27	0.670	0.271	0.094	2.67	0.998	1.29	0.141	0.284	0.568	1.04	0.287	0.292	0.292	0.294

Concentrations are given in mol/l, *: Necessary amount for adjusting pH of the bath to desired value.

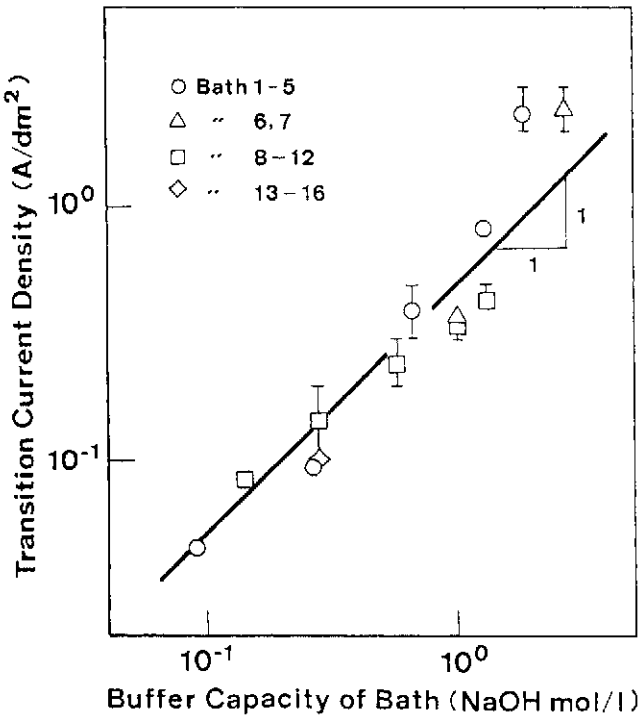

Fig.5 Relationship between transition current density and buffer capacity of the bath.

baths 10, 15 and 16 in which the total metal ion concentrations were greatly different from each other. As the metal ions are normally added to the sulfate bath in a form of metal sulfate, the concentration of sulfate ion which acts as a predominant buffering agent is lower in the baths of low total metal ion concentration unless another sulfate is added. Therefore, lowering the total metal ion concentration results in a decrease in buffer capacity of the bath. Further, lowering the temperature will result in a decrease in the diffusion rate of hydrogen ion to the cathode. Consequently, it is concluded that the transition current density is decreased by changes in plating conditions which bring about the depletion of hydrogen ion in the cathode layer.

2-4 Electrodeposition behavior of Zn-Ni alloys from sulfate baths and the explanation of it based on the hydroxide suppression mechanism [34].

Alloys were electrodeposited on a copper cathode of 2 cm x 2 cm under coulostatic (10 C/cm^2) and galvanostatic conditions at 313 K (40 ºC) from the un-agitated baths (No.10, 13-16 in Table 4) in which either the metal-% of Ni, or total metal ion concentration was varied while the buffer capacity was kept almost constant.

Figure 6 shows the effect of current density on the alloy composition and on the current efficiency for alloy deposition from the bath 10 which has been used as a standard bath in our previous work [32]. Figure 6 also includes the polarization curve measured simultaneously during alloy deposition. Figures 7 and 8 show the same

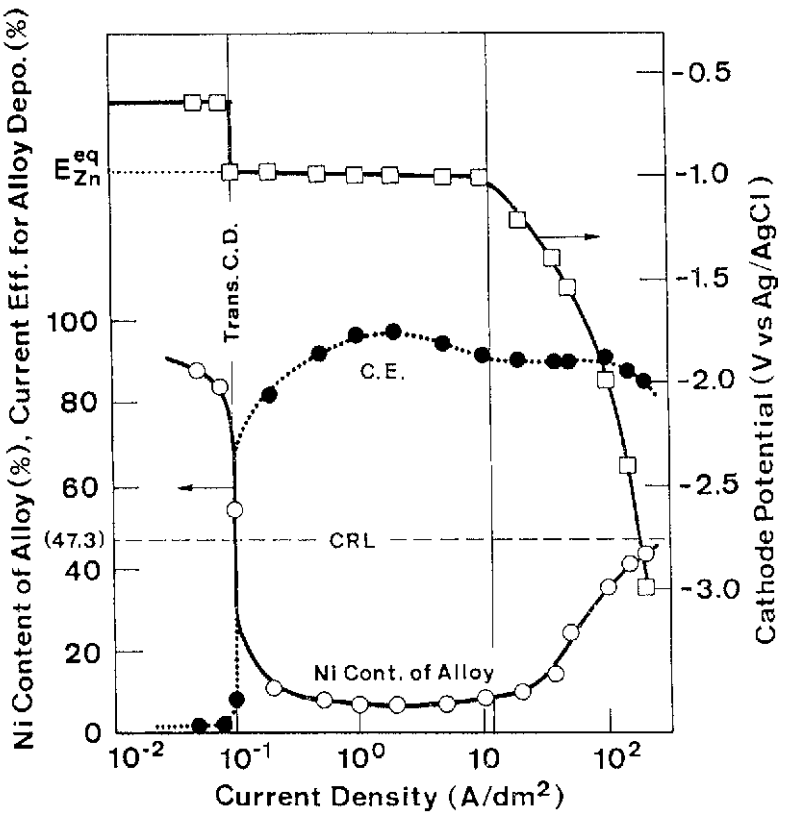

Fig.6 Effect of current density on alloy composition and current efficiency, and the polarization curve during alloy deposition from the bath 10.

relationship as in Fig.6 in the baths having different metal-% of Ni (Bath 13, 14) and in the baths having different total metal ion concentration (Bath 15, 16). The changes in alloy composition and current efficiency for alloy deposition showed the same trend as in Fig.3 although the alloy deposition behavior at higher current densities were revealed in more detail.

From figures 6, 7 and 8, the alloy deposition behavior can be generally divided with respect to the current density into the following four segments as shown schematically in Fig.9: the low current density region I where normal type alloy deposition occurs with poor current efficiency; region II where the preferential deposition of less noble Zn proceeds with considerably higher current efficiency and the alloy composition hardly tends to change; region III where Ni content of the alloys increases with an increase in current density while a relatively high current efficiency for alloy deposition is still maintained; and region IV where Ni content is further increased toward the CRL while the current efficiency for alloy deposition decreases abruptly.

The alloy deposition behavior in region I and its transition to region II have been explained already in 2-3-2. The relationship between the total current density and the partial current densities for the deposition of each metal and hydrogen discharge is shown in Fig.l0 where the results for the baths of 10 and 15 are presented as

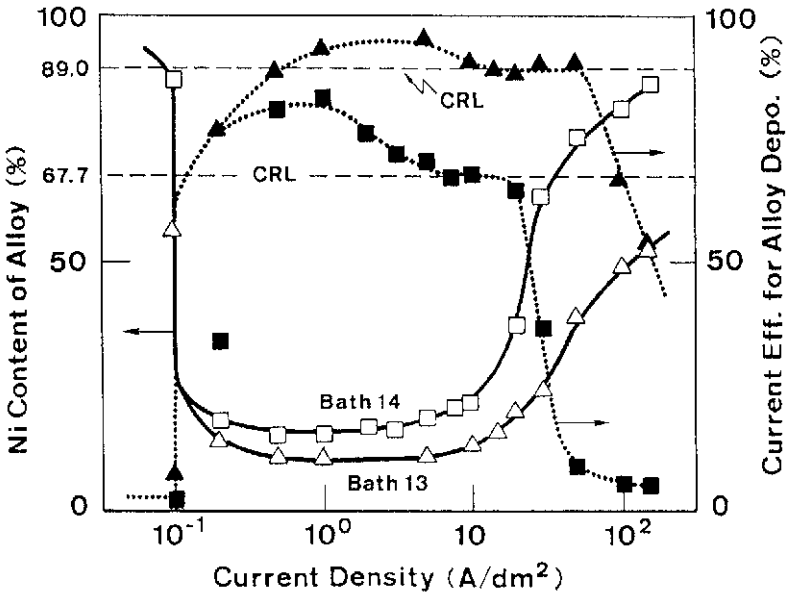

Fig.7 Effect of current density on alloy composition and current efficiency for alloy deposition from the baths having different metal-% of Ni (Bath 13, 14).

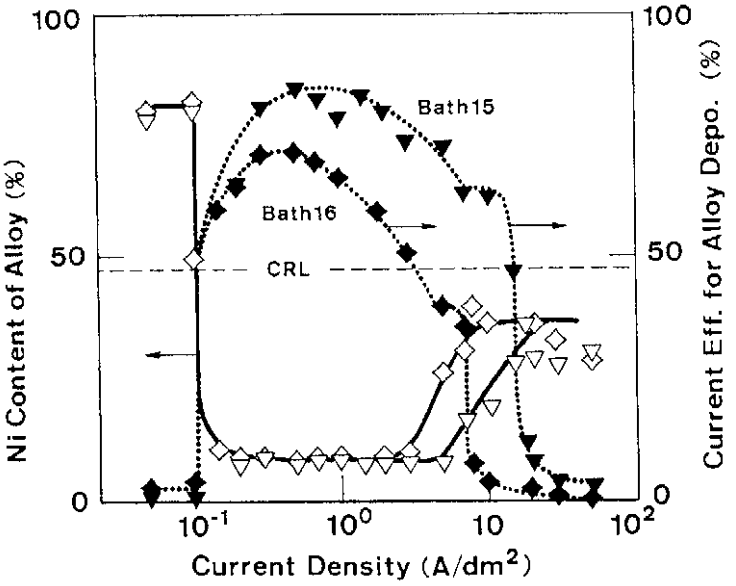

Fig.8 Effect of current density on alloy composition and current efficiency for alloy deposition from the baths having different total metal ion concentration (Bath 15, 16)

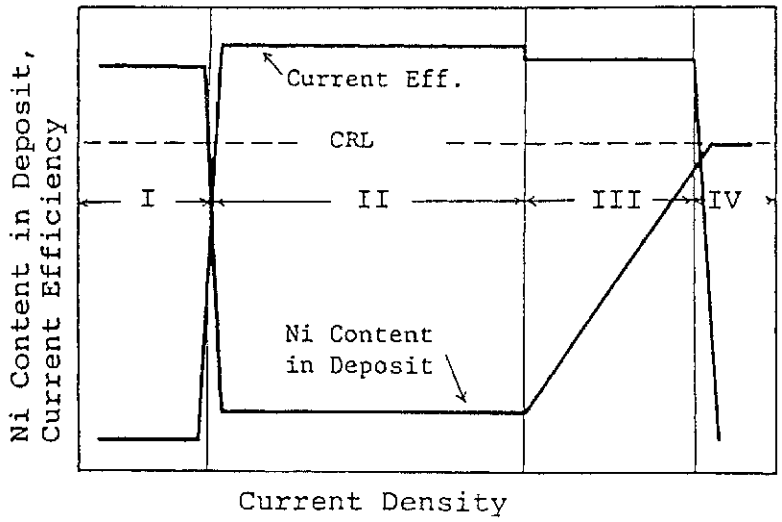

Fig.9 Schematic representation of the alloy deposition behavior.

an example. By using this figure, the explanation of the alloy deposition behavior in region II, III and IV is given below.

In the anomalous codeposition region II, Zn deposits from its hydroxide and behaves as a more noble metal than Ni or hydrogen. The discharge of Ni and hydrogen is, as described previously, greatly affected by the presence of Zn hydroxide whose existence depends on the relative rates of its chemical formation and its electrochemical consumption. The chemical formation rate of Zn hydroxide is determined

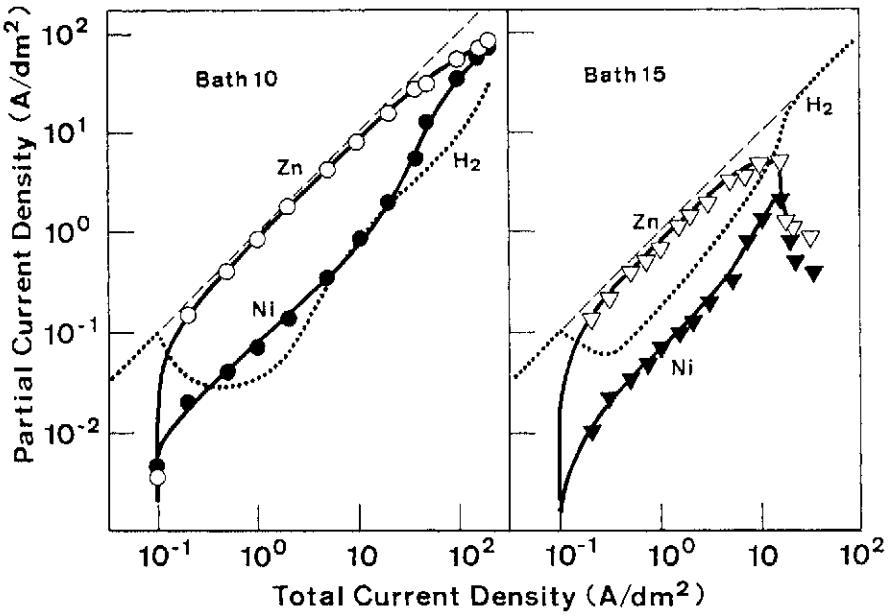

Fig.10 Relationship between total current density and partial current densities for the deposition of each metal and hydrogen discharge in the baths 10 and 15.

by activities of both OH^- and Zn ions on the cathode. Provided that the rate constant of the hydroxide formation is large enough, the formation rate of Zn hydroxide is determined by that of OH^- ions generated by the discharge of Zn hydroxide as well as of hydrogen at the cathode, as long as sufficient Zn ions are supplied from the bulk solution and no Zn deposition under diffusion control begins. On the other hand, the electrochemical consumption rate of Zn hydroxide is exactly equivalent to the deposition current of the Zn. As the OH^- ion formation rate keeps on increasing after the transition, the rate of Zn hydroxide formation always exceeds that of consumption, resulting in the presence of unreduced excess hydroxide. In the presence of a sufficient amount of adsorbed Zn hydroxide, then, the alloy deposition of anomalous type proceeds easily at the potential which is a little less noble than the equilibrium potential of Zn as shown in Fig.6. In this region, as shown in Fig.10, the partial current density of Zn accounts for most of the total current density. The partial current density of Ni is about one tenth of the total current density, indicating almost constant current efficiency of 10 %. The change of partial current efficiency of Zn from 85 to 70 %, for example, results in a little change of Ni content of the alloy from 9.7 to 11.4 %. Thus, the alloy composition hardly tends to change in this region.

With further increase in the current density, as shown in Fig.10, Zn deposition begins to reach its limiting current in preference to Ni deposition because Zn behaves as a more noble metal in the anomalous codeposition region. When Zn deposition begins to reach its limiting current in region III, the chemical formation rate of Zn hydroxide is reduced owing to the decreased concentration of Zn ions available at the cathode while the electrochemical consumption rate still increases gradually toward the limiting current of Zn. With increasing current density, therefore, the amount of adsorbed Zn hydroxide decreases gradually, resulting in the gradual depolarization of the apparent equilibrium potentials of Ni and hydrogen. In addition, as shown in Fig.6, the cathode is further polarized due to the concentration polarization of Zn deposition. This leads to the increase in the driving force for the deposition of hydrogen as well as of Ni. In this region, as shown in Fig.10, the deposition of Ni was facilitated in preference to hydrogen, resulting in the increase in Ni content of the alloys toward the CRL and in the relatively high and constant current efficiency for alloy deposition. According to this discussion, region III, and hence the rising part of the Ni content curve in Fig.9, should be shifted to the left with decreasing Zn ion concentration in the bath, because the limiting current for Zn deposition is attained at lower current density in baths of lower Zn ion concentration. This was evidenced in Figs.6, 7 and 8.

In region IV where the limiting current for Zn deposition is nearly attained (Fig.10), the adsorbed Zn hydroxide is decreased to such an extent as to permit the depolarization of the apparent equilibrium potential of hydrogen to its initial level. Therefore, the predominant hydrogen evolution begins to cause an abrupt decrease in the current efficiency for alloy deposition. In addition, as was evidenced by the abrupt decrease in deposition currents of both metals at high current densities (Bath 15 in Fig.10), the deposits became powdery and could fall away from the cathode. This also contributed to the decrease in the current efficiency for alloy deposition.

2-5 Several experimental results showing the role of iron-group metals in the anomalous type alloy deposition.

2-5-1 Zn-Cd alloy deposition from a sulfate bath [35].

If it is assumed that the properties of iron-group metal described in 2-2 are not responsible for the appearance of anomaly in Zn-iron-group metal alloy deposition, then there arises a possibility that anomalous codeposition might also occur in the simultaneous deposition of Zn with other metals which are more noble than Zn and hydrolyze at a higher pH value. As an example of such a metal, we can find Cd whose standard single electrode potential and critical pH for hydroxide formation are comparable to those of Fe. During Zn-Cd alloy deposition, therefore, Cd must be deposited from its hydrated ion in the presence of Zn hydroxide adsorbed on the cathode.

Table 5 Standard plating conditions for Zn-Cd alloys.

Bath composition		Operating condition	
Zn sulfate	0.92 mol/1 (60 g/l as Zn)	Current density	500 A/m^2
Cd sulfate	0.018 mol/l (2 g/l as Cd)	Temperature	40 °C
Glue	0.1 g/1	Amount of charge	300 kC/m^2
Sulfuric acid	*	Quiescent bath	

* Necessary amount for adjusting pH of the solution to 3.

The alloys were obtained from the sulfate bath under the conditions shown in Table 5. Effects of the bath composition and current density on the alloy composition and on the current efficiency for alloy deposition are shown in Figs.ll and 12. It was found from these figures that normal-type alloy deposition occurred under the conditions studied. The partial polarization curve for each metal deposition was measured using the baths containing Zn and/or Cd. Each single metal bath was prepared by removing the other metal from the alloy plating bath. The results are shown in Fig.13. Figure 14 also shows the changes in alloy composition and current efficiency obtained from Fig.12. As shown in Fig.13, the partial polarization curve for each metal deposition from an alloy plating bath agreed well with that from its corresponding single metal bath. The more noble Cd began to deposit at its equilibrium potential and the deposition rate of Cd rapidly attained its limiting current. When the cathode was polarized to the equilibrium potential of Zn under the diffusion controlled Cd deposition, Zn began to deposit. Thus, this alloy deposition showed typical normal behavior, with the preferential deposition of more noble Cd at noble potentials, as well as rapid decrease in Cd content of the alloys toward the CRL at less noble potentials where Zn was also deposited, the Zn deposition rate increasing as potential was reduced.

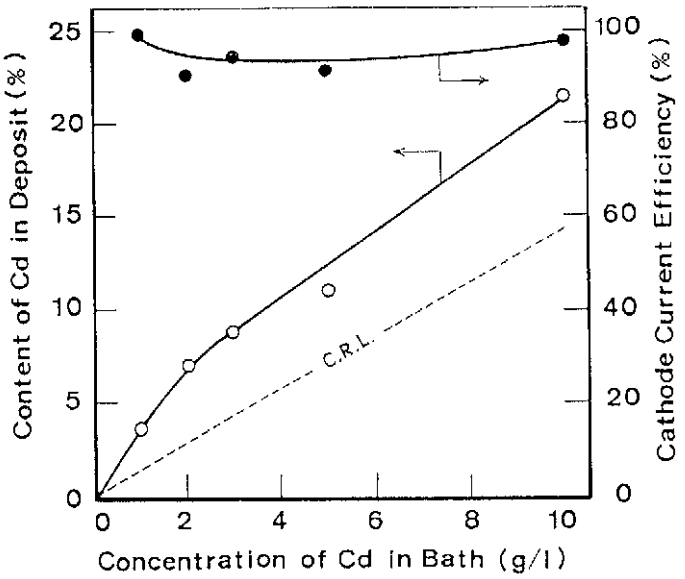

Fig.ll Effect of the concentration of Cd in bath on the alloy composition and on the cathode current efficiency for alloy deposition.

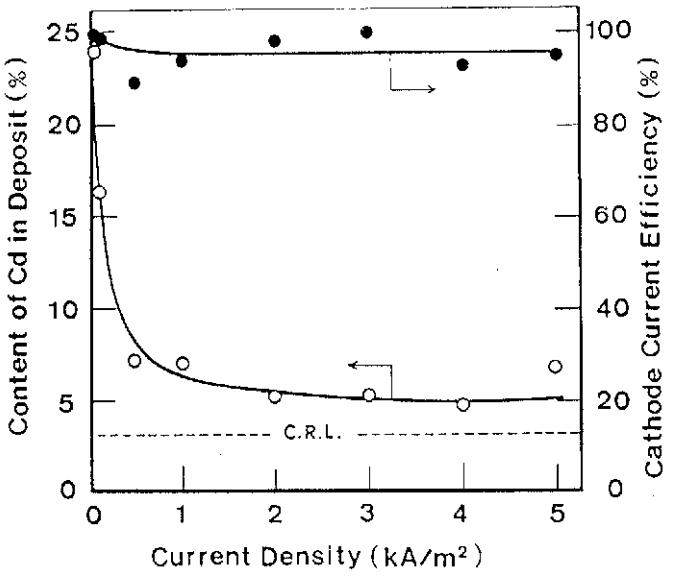

Fig.12 Effect of current density on the alloy composition and on the cathode current efficiency for alloy deposition.

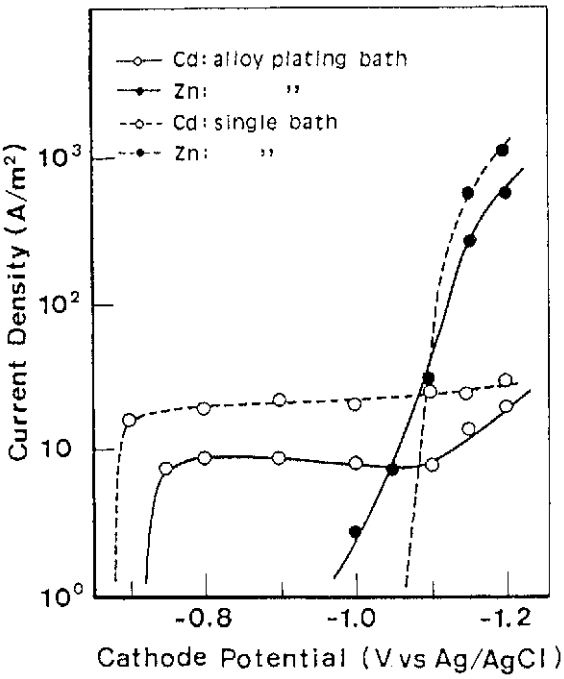

Fig.13 Partial polarization curves for Zn and Cd deposition from the alloy plating bath and from their singles baths.

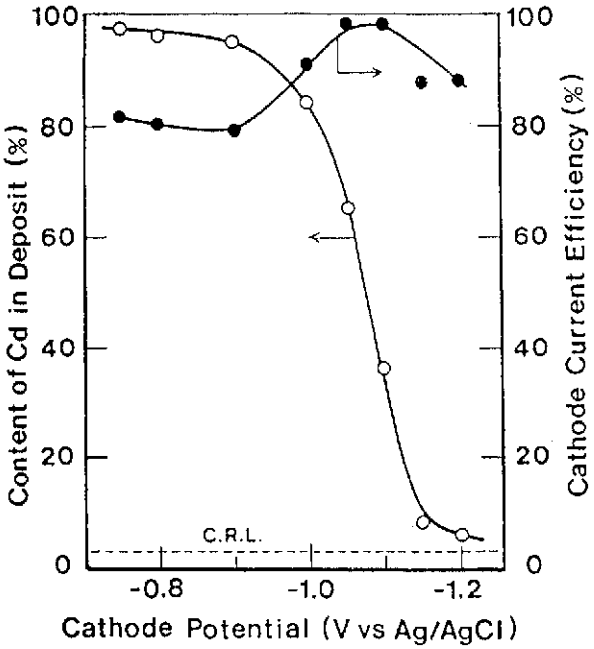

Fig.14 Effect of cathode potential on the alloy composition and on the cathode current efficiency for alloy deposition.

As presented above, no anomalous alloy deposition was observed in Zn-Cd system. This indicates that the properties peculiar to iron-group metal described in 2-2 are essential for the appearance of anomaly in the electrodeposition of Zn-iron-group metal alloys.

2-5-2 Cd-Ni alloy deposition from a sulfate bath [36].

Cd-Ni alloy deposition is one of the best known examples of anomalous codeposition in which electrochemically less noble Cd deposits preferentially. In this case, however, hydroxide formation of the less noble metal cannot be expected because the critical pH for metal hydroxide is lower in Ni than in Cd.

The cathode potential– partial current density curves for each metal deposition from baths containing Ni and/or Cd are shown in Figs.l5, 16 and 17. The alloy plating bath contained 0.9 mol/l of Ni sulfate, 0.1 mol/1 of Cd sulfate, 0.2 mol/l of sodium acetate and an amount of sulfuric acid necessary to adjust the pH of the solution to 3. The metal single bath was prepared by removing Ni or Cd from the alloy plating bath. The measurement was conducted in an un-agitated bath at 30°C.

Cd deposition from its single bath began at its equilibrium potential (-0.65 V vs. Ag/AgCl) and its deposition rate rose almost instantly to its limiting current. This trend was almost the same for Cd deposition from the alloy plating bath. On the other hand, Ni began to deposit from its single bath at a potential which was considerably less noble than its equilibrium value (-0.23 V vs. Ag/AgCl) and its deposition rate rose gradually to the limiting current. This trend is also almost the same as in the alloy plating bath. This indicates that the polarized Ni deposition potential in the alloy plating bath, which is approximately comparable to Cd deposition potential, is not caused

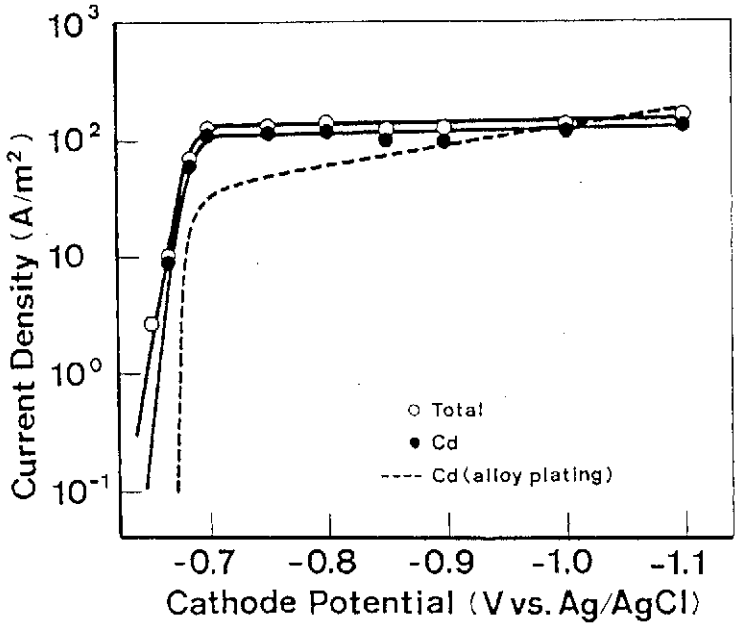

Fig.l5 Polarization curves in Cd single deposition.

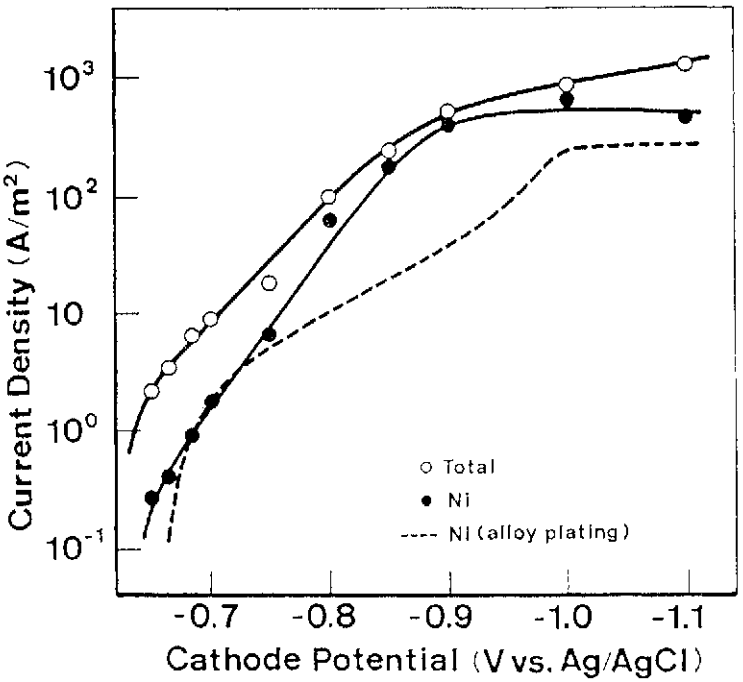

Fig.l6 Polarization curves in Ni single deposition.

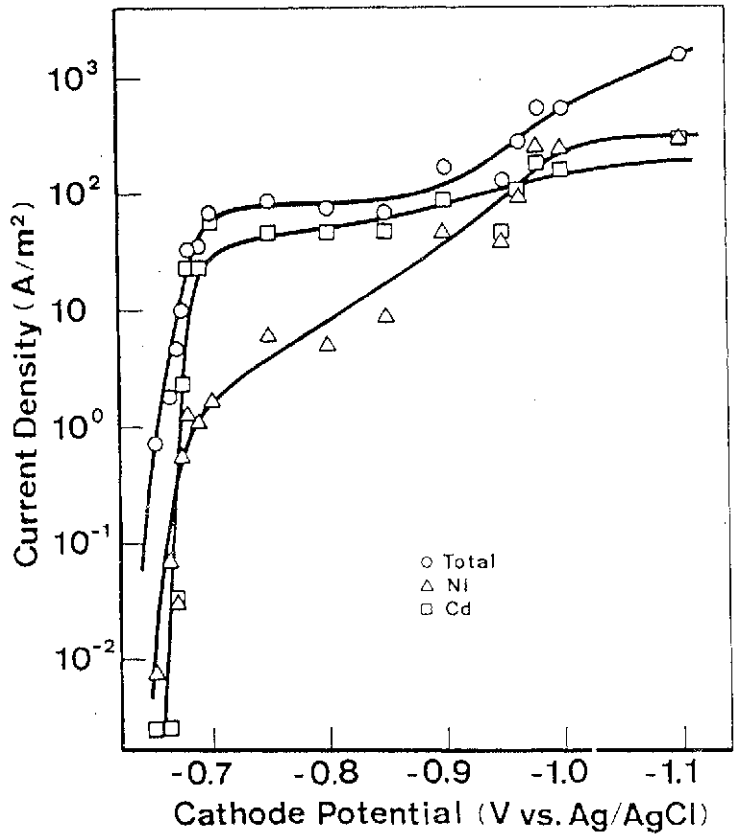

Fig.17 Polarization curves in Ni-Cd alloy deposition.

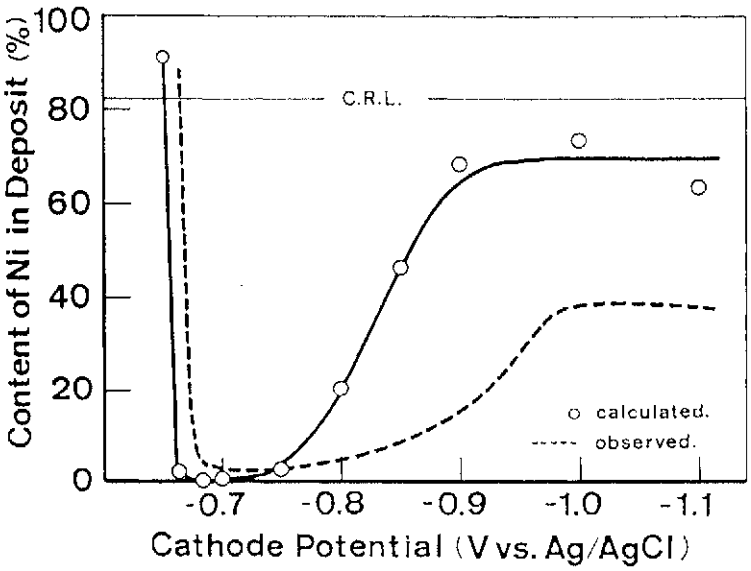

Fig. 18 Alloy composition calculated on the assumption that the rate of alloy deposition is expressed as the sum of the rates of Ni and Cd single deposition.

by interaction with Cd. Therefore, it can be concluded that the preferential deposition of Cd results only from the inherent deposition overpotential of Ni described in 2-2. Figure 18 shows the potential-dependence of the actual alloy composition together with that of the calculated one by superimposing Figs.15 and 16. The trends of both curves agree well, which indicates the validity of the above discussion.

2-5-3 Factors determining the mechanism of anomalous alloy deposition.

As described so far, the properties of iron-group metals in the ionic state play an important role in anomalous alloy deposition. In Cd-Ni alloy deposition, as shown in 2-5-2, the inherent, large, deposition overpotential of Ni was responsible for the anomalous codeposition. On the other hand, in Zn-iron-group metal alloy deposition, the inhibitor such as Zn hydroxide which brought about the additional polarization of iron-group metals was necessary. By combining the electrochemical factor of the single electrode potential of each metal with the chemical factor of critical pH for each metal hydroxide precipitation, we can estimate which of the above two types of anomalous codeposition occurs in a given alloy system.

Table 6 shows the standard single electrode potentials [8] of iron-group metals and of other metals which are less noble than iron-group metals, and which can thus be deposited from hydrated ions at high current efficiency [9]. Table 6 also shows the critical pH for each metal hydroxide precipitation from the solution containing 1 mol/1 of each metal ion [8]. In the electrodeposition of Cd-Ni and Cd-Co alloys, the polarization of iron-group metal due to the adsorbed Cd hydroxide cannot be expected because iron-group metal hydroxide is formed in preference to Cd hydroxide when pH in the cathode layer rises. In this case, however, the differences in single electrode

Table 6 Electrochemical and chemical factors influencing the occurrence of anomalous codeposition in the combined system of more noble iron-group metal with other less noble metal.

element	Ni	Co	Fe	Cd	Zn	Mn
E°(V vs NHE)	-0.25	-0.277	-0.440	-0.403	-0.763	-1.179
pHcri(calculated at 1 mol/1)	6.09	6.30	6.645	6.905	5.48	7.655
pHcri(determined in the bath used)	6.55	6.54	6.44	7.41	5.25	

potentials between both constituents are relatively small, (0.13 and 0.15 V), and the superiority of iron-group metals over Cd in nobility can be canceled only by the inherent deposition overpotential of iron-group metals. In the electrodeposition of Zn-iron-group metal alloys, on the other hand, the differences in single electrode potentials between both constituents are 0.32 - 0.51 V which seem to be too large to be canceled only by the inherent deposition overpotential of iron-group metals. In this case, however, Zn hydroxide is formed at a lower pH than iron-group metal hydroxides. Therefore, the deposition of iron-group metal is further polarized by the adsorbed Zn hydroxide, which results in the cancellation of the superiority of iron-group metals in the electrochemical nobility.

In addition, let us consider the electrolysis of the solution containing Mn and iron-group metal. In this case, the differences in single electrode potentials between both constituents are extremely large (0.74 - 0.93 V) and no Mn hydroxide is formed. Therefore, alloy deposition scarcely occurs from a solution containing these hydrated ions. A complexing agent such as pyrophosphoric acid is required for this alloy deposition [37].

2-5-4 Underpotential deposition of Zn with Ni.

As shown in Fig.6, appreciable amounts of Zn-Ni alloys are deposited in the low current density region I where cathode potential was not polarized thermodynamically to permit Zn deposition. This means that Zn deposition nevertheless occurs at potentials which are more noble than its equilibrium value. The mechanism which permits this interesting underpotential deposition of Zn remains to be provided. In anomalous Zn-iron-group metal alloy deposition, as already mentioned, the properties of iron-group metal in the ionic state play an important role but those in the metallic state may make no contribution. However, there still is a possibility that the properties of iron-group metals in the metallic state may be involved in the underpotential deposition of Zn with Ni because this phenomena shows, as explained later in detail, the main feature of induced codeposition where properties in the metallic state play an important role.

Table 7 shows the experimental conditions used. The extremely low concentration of Zn in the bath, compared to iron-group metal, was adopted in order to co-deposit as much Zn as possible. The temperature

Table 7 Experimental conditions for the study of the underpotential deposition of Zn with iron-group metals.

Bath composition		Operating condition
Zn sulfate	0.025 mol/l	Cathode potential -0.6 ~ -1.3 V vs Ag/AgCl
Iron-group metal sulfate	0.5 mol/l	Temperature 5 ~ 80 °C
		Amount of charge 100 kC/m^2
Sulfuric acid	*	Quiescent bath

* Necessary amount for adjusting pH of the solution to 3.

was varied over a wide range from 5 to 80°C because the deposition overpotential of iron-group metals depends greatly on the temperature and almost disappears at elevated temperatures [10]. Although the experiments were conducted with every combination of Zn and iron-group metal, only the results for Zn-Ni system are presented since the results showed the same trend in each alloy system.

Figure 19 shows the partial polarization curve for each metal deposition from its single bath at different temperatures. At all temperatures studied, Zn deposition began at its equilibrium

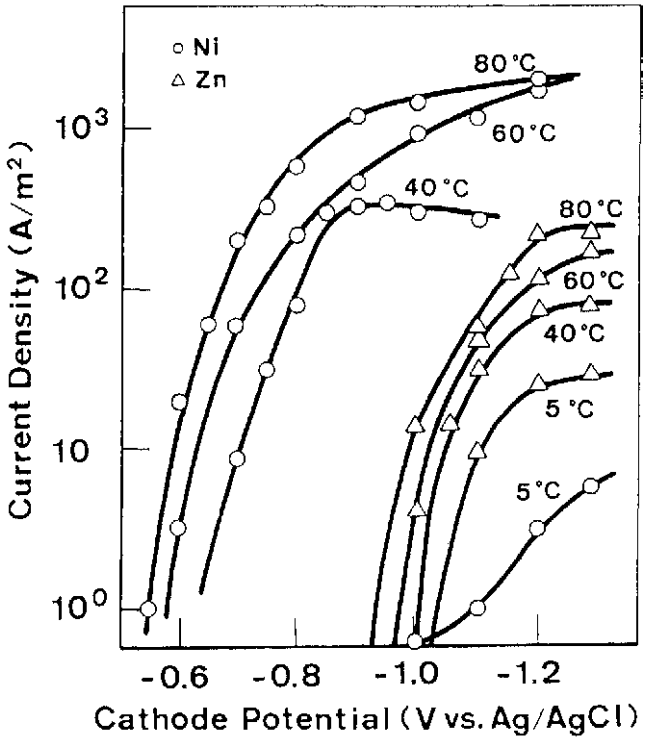

Fig.19 Effect of bath temperature on the partial polarization curves of Ni and Zn for electrodeposition from their single solutions.

potential, although the limiting current for Zn deposition increased with a rise of temperature. In Ni deposition, on the other hand, the deposition potential, which was greatly polarized at 5ºC, shifted at 80 °C approximately to its equilibrium value.

Zn-Ni alloys were electrodeposited at two different temperatures, 40 and 80ºC. At 40ºC Ni still exhibited a considerable inherent overpotential for the initiation of deposition, but at 80ºC its inherent deposition overpotential almost disappeared. A comparison between the partial current densities for each metal deposition from a single bath and those from the alloy plating bath is shown in Figs.20 and 21 for results at 40ºC and 80 ºC, respectively. From Fig. 20, Ni deposition was depressed considerably in the alloy plating bath, which simply indicated the main feature of anomalous codeposition. Zn deposition, on the other hand, occurred from the alloy plating bath at noble potentials where no Zn deposited from the single bath. The underpotential deposition of Zn was thus observed in the alloy deposition. At 80 ºC where the inherent deposition overpotential of iron-group metal almost disappeared, Ni began to deposit from the alloy plating bath at the same potential as in the single bath, and at this temperature the current for underpotential deposition of Zn was greatly increased. As shown in Fig.22, Auger electron spectroscopic analysis of the deposits obtained at underpotential (-0.75 V vs. Ag/ AgCl) and overpotential (-1.10 V vs. Ag/AgCl) conditions revealed metallic Zn in both deposits, and there was no evidence that Zn hydroxide formed on the cathode was incorporated into the deposit.

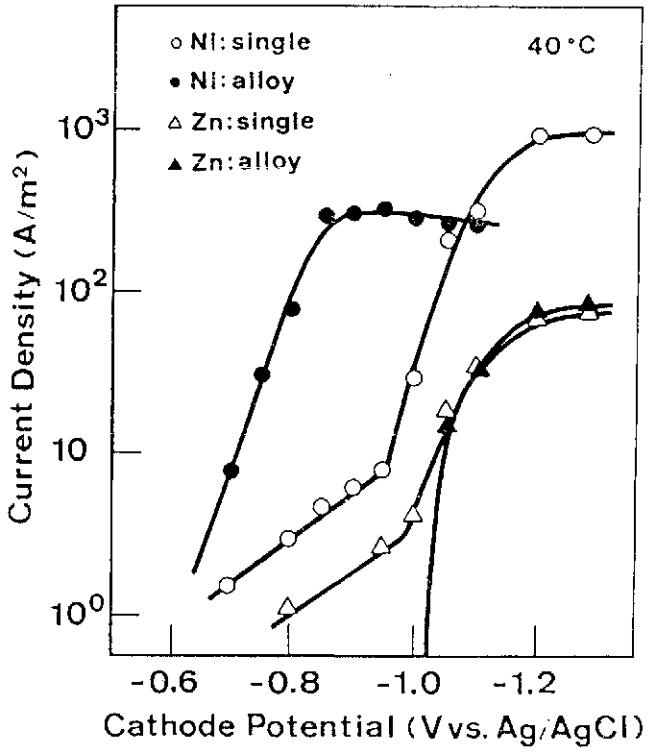

Fig.20 Comparison between partial polarization curves of Ni and Zn during electrodeposition of Zn-Ni alloy and those of the single metals at 40 °C.

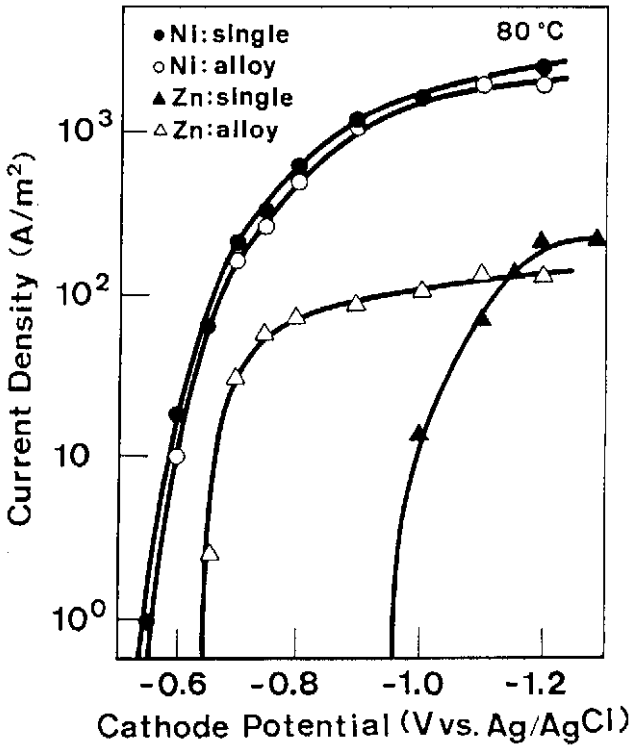

Fig.21 Comparison between partial polarization curves of Ni and Zn during electrodeposition of Zn-Ni alloy and those of the single metals at 80 °C.

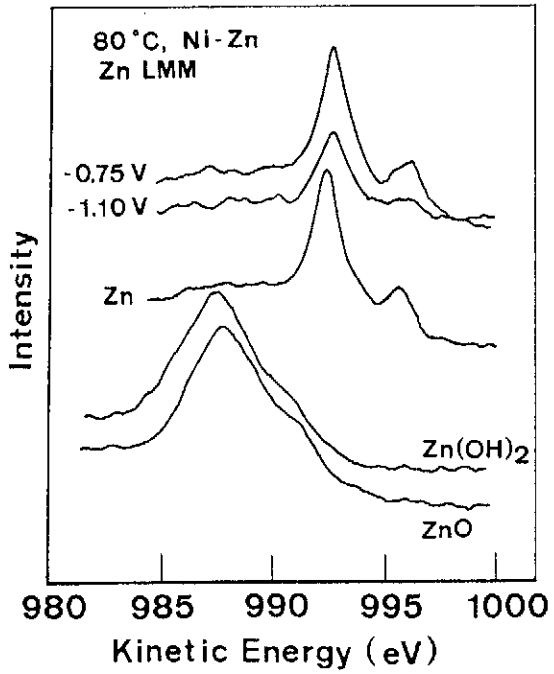

Fig.22 Auger electron spectra of Zn (LMM auger process) in pure Zn metal, $Zn(OH)_2$, ZnO and electrodeposited Zn-Ni alloys.

Further, the electrodeposition of Zn alloys with other metals was examined in connection with the underpotential deposition of Zn. Figure 23 compares the partial polarization curves for Zn deposition from Zn-Cd and Zn-Cu alloy plating baths, Zn-Ni alloy, and Zn single baths. The partial polarization curves for Zn deposition from Zn-Cd and Zn-Cu alloy plating baths corresponded closely to that from the Zn single bath.

As presented above, the underpotential deposition of Zn occurred only in the presence of iron-group metals and was facilitated when conditions permitted a decrease in the inherent deposition overpotential of iron-group metals to bring about their easy deposition. This appears to be the same phenomena as the induced codeposition of reluctant metals, in which the properties of iron-group metal in the metallic state play an important role in electrodeposition of the alloys at significant current efficiency [27]. In the induced type alloy deposition, however, the reluctant metal ion can reasonably be reduced to a metallic state in the presence of a catalyst, because the thermodynamic driving force for its deposition exists. On the other hand, the underpotential deposition of Zn ion occurs in a potential region where no thermodynamic driving force exists. Therefore, it seems to be impossible to apply the mechanism of induced type alloy deposition directly by explaining that the atomic hydrogen held on freshly deposited iron-group metal reduces Zn hydroxide to metallic Zn.

In the electrodeposition of certain metals on different metal

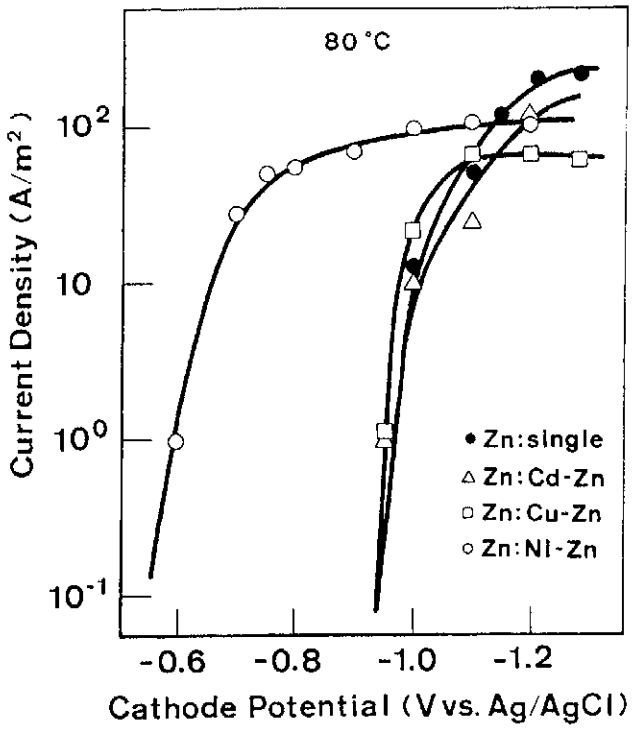

Fig.23 Partial polarization curves of Zn during the electro-deposition of single Zn, Cd-Zn, Cu-Zn and Ni-Zn alloys.

substrates, the equilibrium potential of the metal to be deposited is shifted infinitely into the positive region because the activity of the metallic phase is zero before it begins to deposit. Consequently, in the potential region which is more noble than the equilibrium value calculated under the condition that the metal phase activity is unity, metal deposition should be possible, even in a trace quantity, until the deposited metal comes to exhibit the activity which corresponds to the given potential. Since the quantity of deposited metal is of course too small to be detected by chemical analysis, no massive metal deposition is recognized in practice in the underpotential region. If the codepositing iron-group metal brings about a situation which permits the activity of deposited Zn on the progressively formed cathode surface to be maintained at a value not exceeding the one corresponding to the given potential, it becomes thermodynamically possible to explain the large amount of underpotential deposition as shown in Fig.21.

As described above, the properties of iron-group metal in a metallic state seem to be concerned in the underpotential deposition of Zn, although the mechanism is entirely obscure at the moment.

3. Feasibility study for the development of a Zn-Ni alloy plating process.

3-1 General conditions which yield alloys for practical use.

Regions II and III are preferred for commercial plating because of their high current efficiency as presented in 2-4. The relationship between alloy composition and current efficiency for each metal or alloy deposition was obtained from Figs.6, 7 and 8 and shown in Figs.24 and 25. At low Ni contents of the alloys which corresponded to the region II, partial current efficiency of Ni was low and lay in a narrow range from 5 to 15 % although high values of current efficiency for alloy deposition were observed because of high partial current efficiencies of Zn. With increasing Ni content of the alloy, the partial current efficiency for Zn deposition decreased proportionately, whereas that for Ni increased. This permitted the almost constant and relatively high current efficiency for alloy deposition in region III.

In the anomalous codeposition regions Il and III, as mentioned previously, Zn behaves as a more noble metal than Ni, and Zn deposition reaches its limiting current in preference to Ni with increasing current density. When the limiting current for Ni deposition is attained, the composition of the alloy becomes identical to that of the bath (CRL) because both limiting currents for metal deposition are attained. The limiting Ni content of the alloy is thus given by the metal-% of Ni in the bath. As shown in Figs.24 and 25, however, this limiting Ni content is scarcely reached in practice, especially in low Zn ion concentration baths (Baths 14, 15, 16), because of the abrupt decrease in current efficiency due mainly to powdery deposition in region IV. It was found from Figs.24 and 25 that the current efficiency for alloy deposition began to decrease abruptly when the partial current efficiency of Zn decreased to become

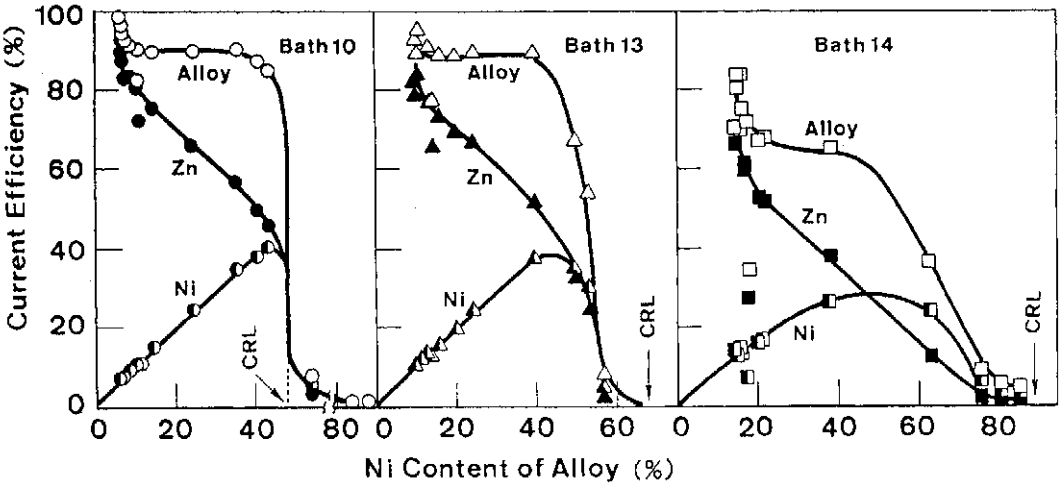

Fig.24 Relationship between alloy composition and current efficiency in baths 10, 13, 14 (see Table 4).

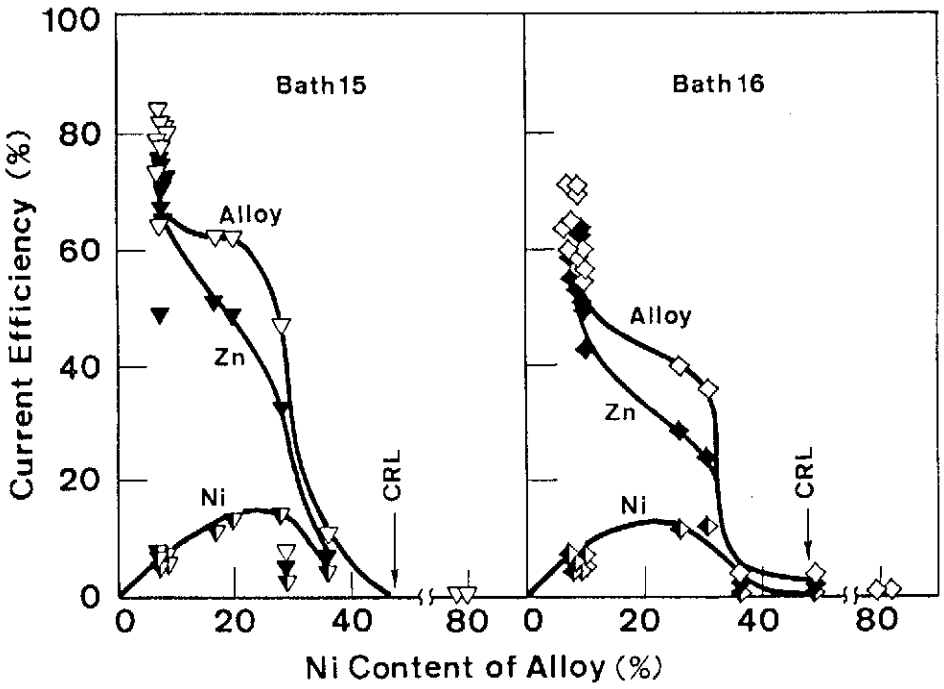

Fig.25 Relationship between alloy composition and current efficiency in baths 15 and 16.

identical to the increasing partial current efficiency of Ni. This means that the deposition current of Ni increased immediately to become identical to that of Zn and the deposits become powdery when Zn deposition reaches its limiting current. When both metal deposition currents are identical to each other, the alloy composition should be identical to the CRL of the bath containing equimolar amounts of each metal ion. The alloy composition at this point (47.3 % Ni) seems to present the maximum Ni content of the alloy obtainable with acceptably high current efficiency.

As mentioned above, alloys of relatively high Ni content can be obtained with considerably high current efficiency in region III. However, region II is considered to be most favorable because the alloy composition hardly changes over a wide range of current density. The most corrosion resistant Zn-Ni alloys contain 10 - 16 % Ni and consist of single gamma phase [38]. Although the Ni content of the alloys is rather low in region II, alloys of these compositions can be obtained by increasing the metal-% of Ni in the bath while maintaining the Zn ion concentration at relatively high level [39].

Region II is bounded by the transition current density and the current density at which Zn deposition begins to reach its limiting current. The transition current density is unequivocally determined by the buffer capacity of the bath as concluded in 2-3-3, while the current density at which Zn deposition begins to reach its limiting current depends on the degree of Zn ion depletion in the cathode layer. Therefore, region II broadens when the conditions favor high depletion of hydrogen ion and low depletion of Zn ion in the cathode diffusion layer.

Besides alloy composition and current efficiency which are the

most important factors to be considered, surface appearance of the deposit, stability and throwing power of the bath, energy or voltage efficiency for plating and anodic dissolution behavior of metal anodes are also important in commercial plating. Taking all these factors into consideration, electrodeposition of alloys was conducted on the basis of the above discussion of the conditions yielding alloys for practical use. Results and discussion are given below.

3-2 Electrodeposition of alloys from the sulfate bath.

3-2-1 Effect of pH on the width of region II in the simple sulfate bath which is free from organic acid.

The transition current density is lower in baths having lower buffer capacity, resulting in a wider current density range II. Figure 26 shows the calculated pH-buffering characteristics of the standard alloy plating bath (Bath 10 in Table 4) when the initial pH is varied. As is evident from this figure, the dissociation of HSO_4^{2-} to SO_4^{2-} (pK=1.99) is the major buffering reaction in the sulfate bath. Figure 27 shows the effect of bath pH on alloy deposition behavior when sodium acetate was removed from bath 10, using plating conditions as described in 2-4. As is evident from these figures, the transition current density becomes lower and then region II is broadened in baths having higher pH because increasing pH greatly decreases the buffer capacity of the bath. In the bath of pH 4.5, region I

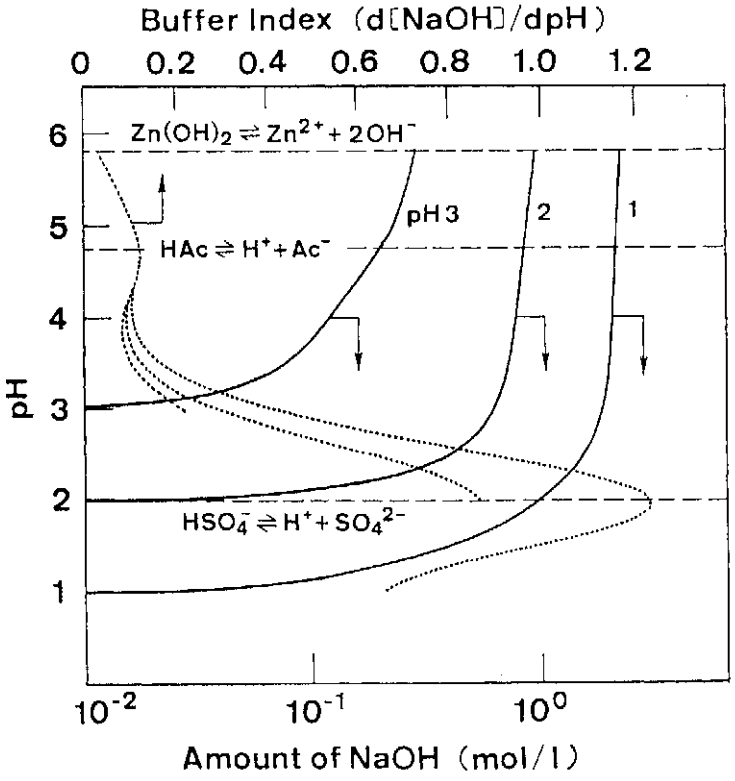

Fig.26 Theoretical titration curves and buffer indices when initial pH is varied in bath 10.

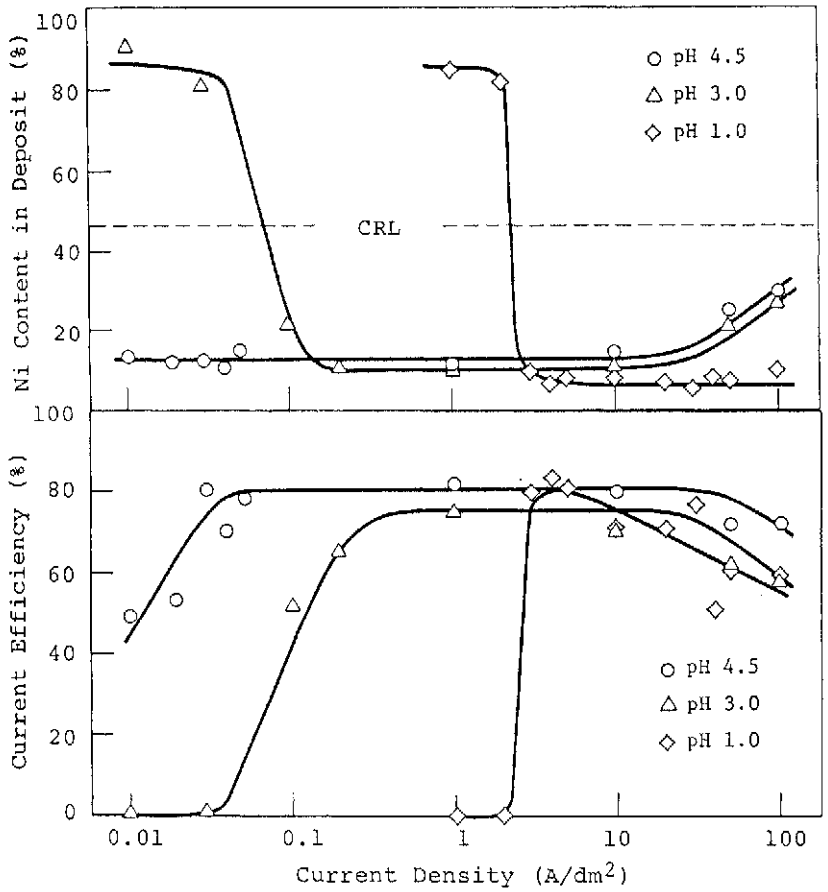

Fig.27 Effect of current density on the Ni content of the deposit and on the cathode current efficiency for alloy deposition from the sulfate bath with various pH values.

disappeared completely because of too small transition current density and alloys whose composition (12 % Ni) corresponded to the single gamma phase composition were obtained consistently in region II.

3-2-2 Long term plating.

In Zn-Ni alloy deposition studies presented in the previous sections, coulostatic plating was conducted at 10 C/cm^2. This amount of charge gives the deposit ca. 5 μm in thickness which is normally adopted in the production of alloy plated steel sheet by steel manufacturers. In the commercial plating of small components, on the other hand, thicker film, ca. 15 pm, is desired. An alloy composition change with prolonged electrolysis would therefore give rise to a problem.

Therefore, alloys were deposited at two different amounts of charge (10 and 30 C/cm^2) from the same bath of pH 4.5 as used in the plating study shown in Fig.27. The alloy deposition behavior in the two cases is compared in Fig.28. It is obvious from this figure that the changes in alloy composition and current efficiency are negligible after prolonged electrolysis in region II.

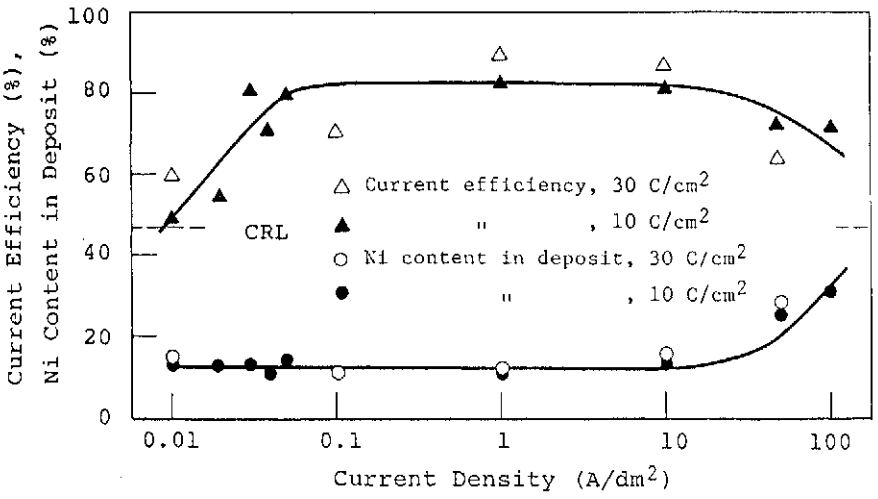

Fig.28 Effect of electrolysis-duration on alloy composition and on the cathode current efficiency for alloy deposition at various current density.

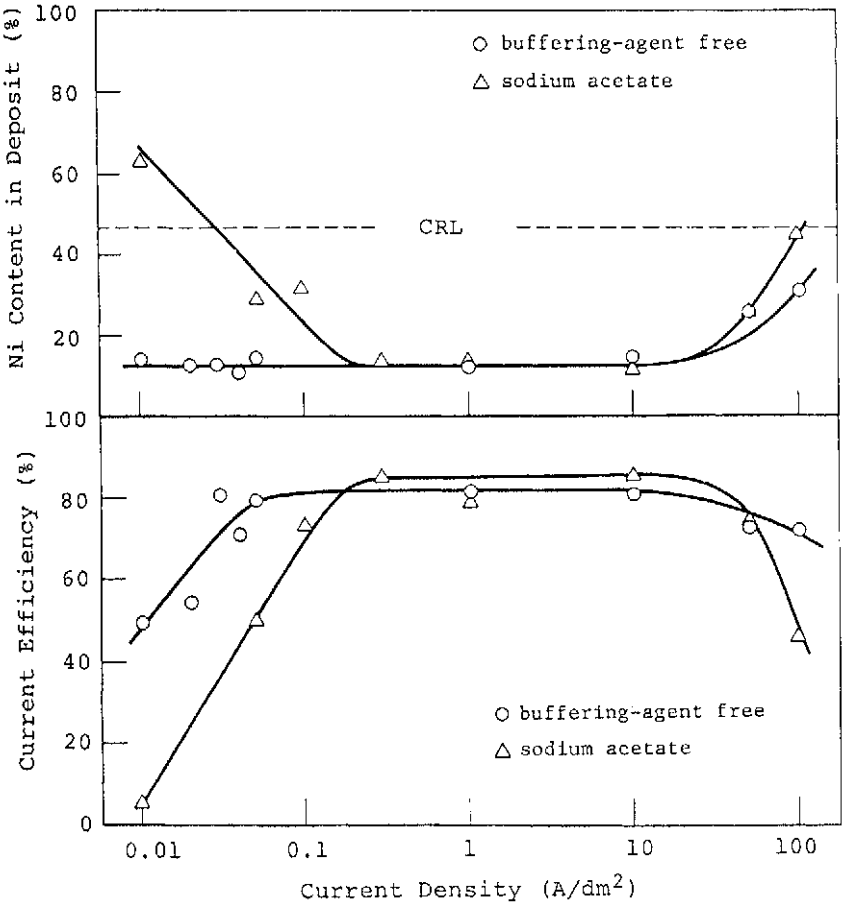

Fig.29 Effect of sodium acetate on alloy composition and on the cathode current efficiency for alloy deposition.

3-2-3 Electrodeposition from baths containing different organic or inorganic acids.

As shown in Fig.28, alloys of stable composition can be obtained from the bath of pH 4.5 over a wide range of current density. However, baths having high value of pH might easily suffer from hydrolysis of metal ions. Then, certain organic or inorganic acids which act either as buffering agents or complexing agents could be introduced into the bath to make it more stable. These acids might also improve the conductivity of the bath to reduce cell voltage.

Alloys were electrodeposited from the baths of pH 4.5 which contained 0.5 mol/1 of each metal ion, and, organic or inorganic acids in the form of sodium acetate, sodium citrate, boric acid or succinic acid. Concentration of these acids was 0.25 mol/1 for succinic acid and 0.5 mol/1 for others. A lower concentration of succinic acid had to be adopted because of its low solubility. The amount of charge for electrolysis was 10 C/cm^2. The alloy deposition behavior in each bath is summarized in Figs.29 and 30. Figure 29 also contains corresponding curves for an organic acid-free bath taken from Fig.28 for comparison.

Addition of these acids increased the transition current density

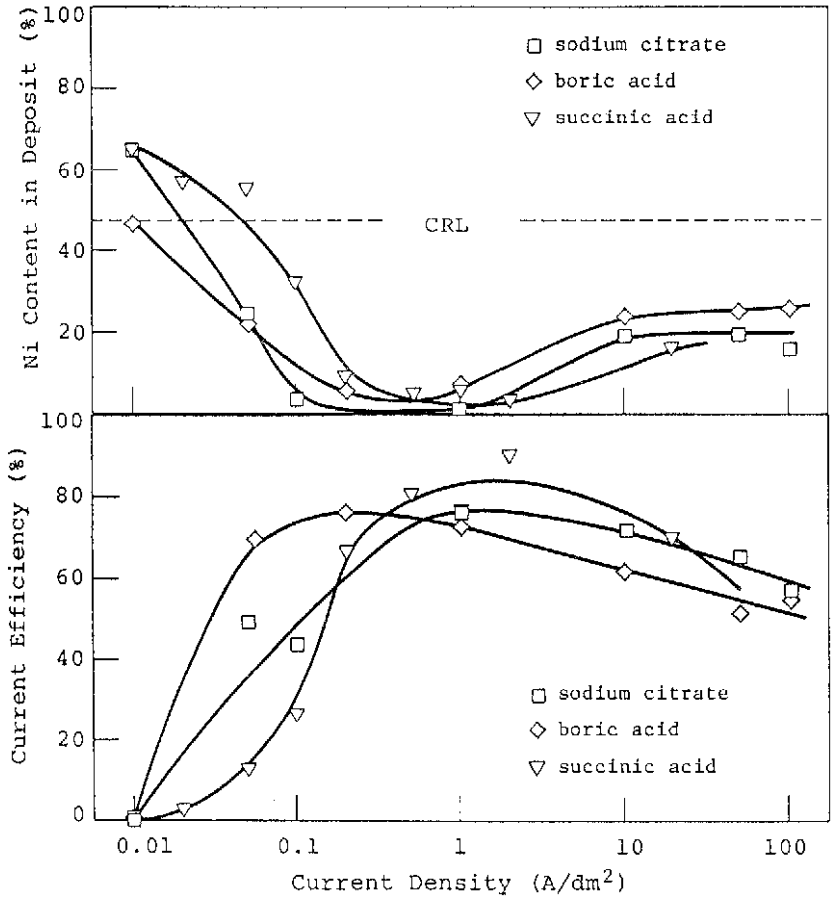

Fig.30 Effect of sodium citrate, boric acid or succinic acid on alloy composition and on the cathode current efficiency for alloy deposition.

probably because of an increased buffer capacity or rise in critical pH for metal hydroxide precipitation due to stable metal complex formation. When the bath contained sodium citrate, boric acid or succinic acid (Fig.30), the rising part of the Ni-content curve (region III) also shifted to the left, resulting in a narrower region II. In addition, the Ni content of the alloys obtained in region II decreased to such an extent that no single gamma-phase formation could occur. In the bath of pH 4.5, as shown in Fig.26, the dissociation of acetic acid (pK=4.74) is the major buffering reaction and the solution has the largest resistance against change in pH at pH 4.74 which is a little lower than the critical value for Zn hydroxide precipitation. Of the acids examined, therefore, sodium acetate which acts not as a complexing but as a buffering agent is most preferable because a relatively small amount of it may stabilize the bath to some extent without affecting the width of region II too much.

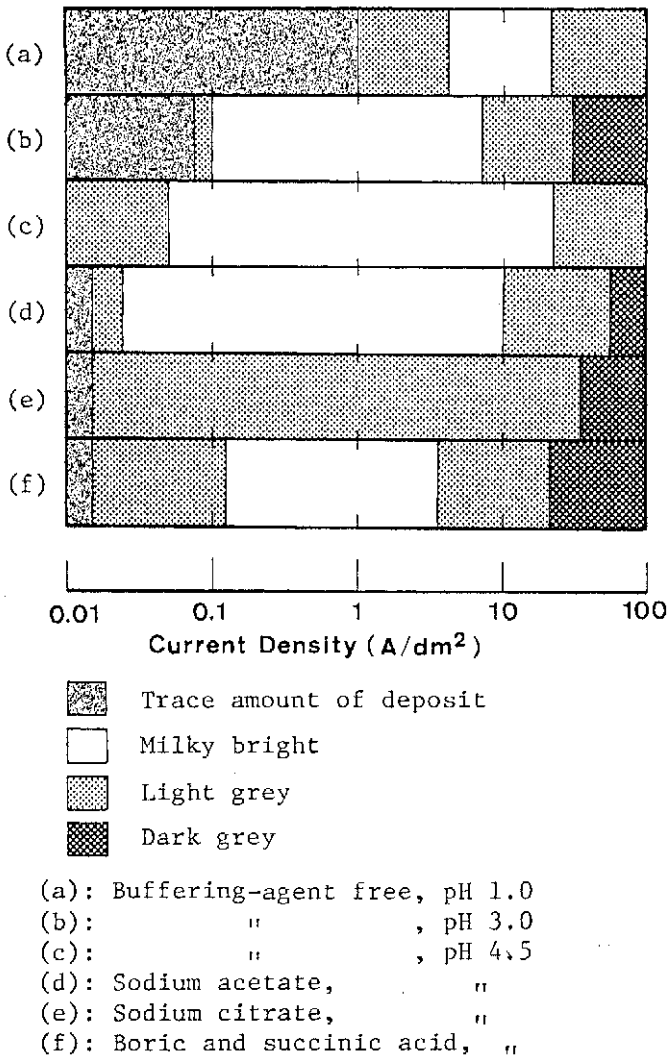

Fig. 31 Schematic representation of the appearance of the deposits obtained from the various types of sulfate baths.

3-2-4 Surface appearance of the deposit.

The surface appearances of the alloys deposited from various sulfate type plating baths examined here are summarized and presented schematically in Fig.31 as a function of the current density. Photo.l shows the typical appearance in each current density region in Fig.31.

In general, milky bright deposits are obtained in region II where anomalous alloy deposition proceeds with high current efficiency. As the current density is increased, the deposits change gradually from light (region III) to dark gray (region IV). Since the deposits having satisfactory surface appearance are obtained only in region II, either organic acid-free or sodium acetate-containing baths yield preferred deposits over a wide range of current density.

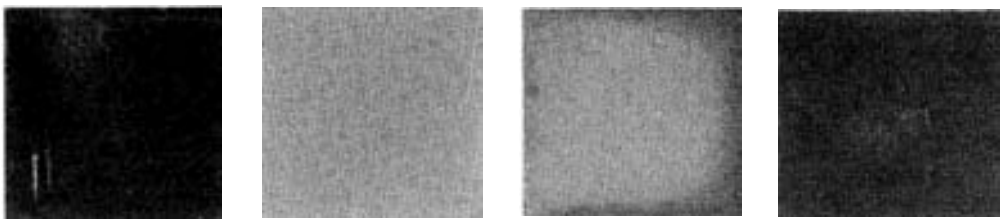

a) trace amount of deposit
b) milky bright deposit
c) light grey deposit
d) dark grey deposit

Photo. l Typical surface appearance of deposits.

3-3 Electrodeposition of alloys from the chloride bath.

3-3-1 Electrodeposition behavior and surface appearance of the alloys.

The sulfate bath, which is basically a mixture of metal sulfate solutions, has been employed in the production of Zn-Ni alloy plated steel sheet by steel manufacturers. In this commercial plating, continuous high-speed operation at high current density has been adopted from the viewpoint of production efficiency but strict control of operating conditions is necessary. Therefore, another type of bath will be preferably for use in practical operation by electroplaters who carry out batch plating of small components. Zn-Ni alloys containing 5 - 85 % Ni (preferably 10 - 20 % Ni) can be obtained from cyanide, ammoniacal, pyrophosfate and alkaline zincate baths and from weakly acidified sulfate/sulfamate-, chloride- or acetate-base baths. Alkaline baths are especially used to obtain Zn-rich alloys while the acidic baths such as sulfate and chloride baths are mainly adopted to obtain Zn-rich but also Ni-rich alloys [40]. Of these baths for Zn-Ni alloy plating, the chloride bath was selected for further study because it seemed to have favorable properties for commercial plating including good anode dissolution and high conductivity to yield high energy efficiency.

Alloys were electrodeposited at various current densities from a simple chloride bath containing 0.5 mol/1 of each metal chloride. pH of the solution was adjusted to 1.0, 3.0 or 4.5 with hydrochloric acid. Operating conditions were the same as described in 2-4 or 2-3-1. The alloy deposition behavior and surface appearance of the deposits

are shown in Figs.32 and 33, respectively.

In all baths examined, as shown in Fig.32, the transition from a normal to an anomalous type occurred at almost the same current density, 0.2 A/dm^2, showing little dependence of transition current density on bath pH. At current densities above the transition, alloys of almost constant Ni content from 10 to 15 % were deposited with high current efficiency in the bath of pH 1.0, which was just the same trend as observed in the sulfate bath. On the other hand, Ni content was varied considerably from 15 to 40 % when pH was increased to 3.0 and 4.5, although relatively high current efficiency was observed even in the normal codeposition region I.

As shown in Fig.33, milky bright deposits are obtained when the alloys contained 10 - 20 % Ni. As the Ni content increased to exceed 20 %, the surface appearance of the deposits became gray.

As mentioned above, the bath of pH 1 is preferred amongst the chloride baths examined because it has the widest range of current density which permits the deposition of milky bright alloys consisting of single gamma phase.

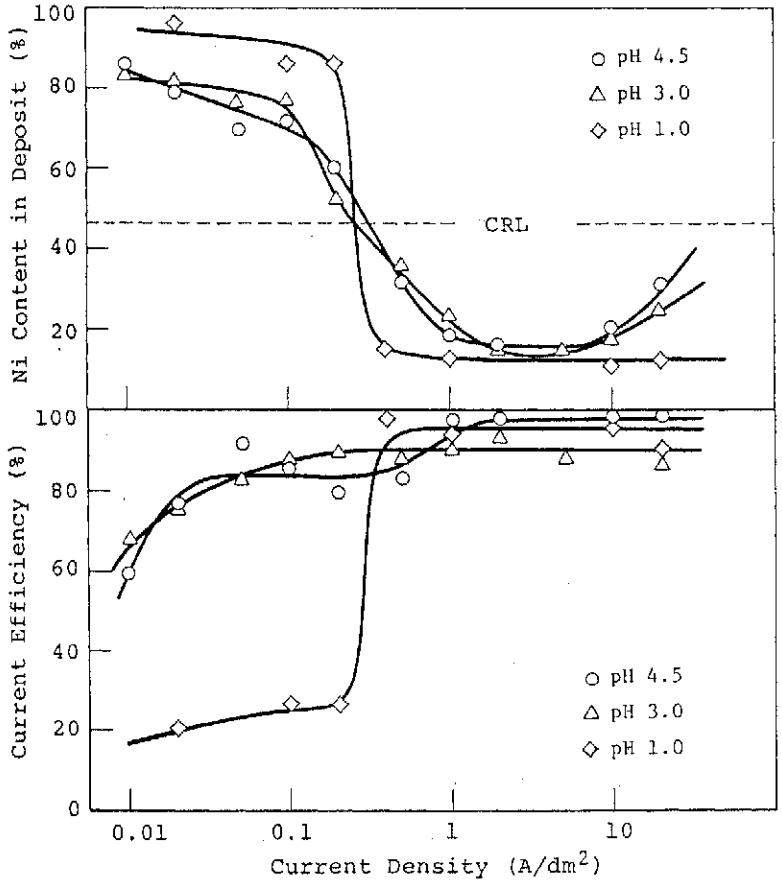

Fig.32 Effect of current density on the Ni content in the deposits and on the cathode current efficiency for alloy deposition from the chloride baths with various pH values.

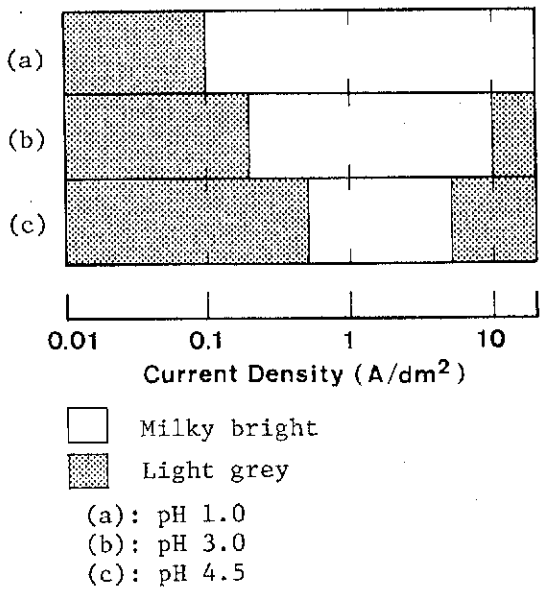

Fig.33 Schematic representation of the appearance of the deposits obtained from the chloride baths with various pH values.

3-3-2 Comparison with the sulfate bath.

In an attempt to obtain alloys for practical use from sulfate and chloride baths, it was found that a simple sulfate bath of pH 4.5 and a simple chloride bath of pH 1.0 are preferred. Deposition behavior of the alloys from these two baths is compared in Fig.34. The current density range which gives stable alloy composition and high current efficiency is wider in the sulfate bath than in the chloride bath because the transition current density is extremely small in the sulfate bath. When the chloride bath is compared with the sulfate bath containing sodium acetate (Fig.29), however, the chloride bath is preferable because the current efficiency is higher while the transition current density is similar.

Alloy deposition behavior in a chloride bath is different from that in a sulfate bath in the following two respects: the transition current density is almost independent of the bath pH; and the current efficiency for alloy deposition is very much higher in the normal codeposition region.

Despite having the same value of bath pH, the transition occurred at a higher current density in the chloride bath than in the sulfate bath as shown in Fig.34. This was probably caused by an increased critical pH for Zn hydroxide precipitation. Since chloride baths examined here contained no pH buffering agent, change in buffer capacity of the bath was small when pH was varied. Therefore, transition current density was hardly affected by pH of the bath.

In the discussions presented so far on alloy deposition from the sulfate bath, no reference has been made concerning the situation that the inherent large deposition overpotential of iron-group metal decreased in the presence of a catalyst. It is known that Cl ion acts as such a catalyst for Ni deposition [41]. Therefore, the anomalous

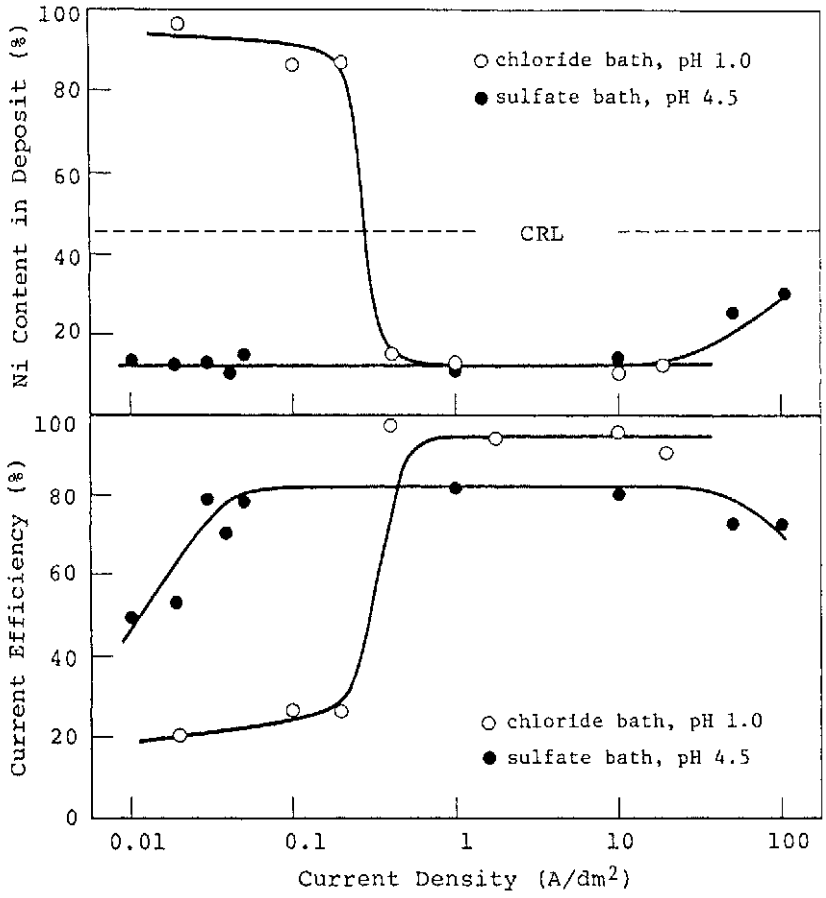

Fig.34 Comparison of alloy composition and cathode current efficiency for alloy deposition between the chloride bath and sulfate baths.

codeposition will occur only with difficulty when the deposition potential of Ni is depolarized almost to its equilibrium value in the presence of large amount of Cl ion. It has been already mentioned in 2-5-4 that the underpotential deposition of Zn with Ni occurred with relatively high current efficiency when conditions permitted low inherent overpotential for Ni deposition. Therefore, either rising temperature or introducing Cl ion into the bath leads to the normal type alloy deposition with relatively high current efficiency.

3-4 Dissolution behavior of anodes in both sulfate and chloride baths.

3-4-1 Dissolution efficiency of soluble metal anodes.

In the case that an insoluble anode is used for plating, evolution of gas such as oxygen or chlorine normally occurs there at very noble potentials, resulting in operation at low energy efficiency due to high cell voltage, and, in the depletion of metal ions in the bath, giving difficulty during long term service. To avoid these problems, the metal to be plated should be used as a soluble anode. In the electrodeposition of alloys of fixed composition, however, the partial current efficiency for each metal deposition is of course less

Table 8 Experimental conditions for the measurement of anode current efficiency.

Bath composition		Electrolysis condition	
Sulfate bath:		Current density	0.4 - 50 A/dm^2
Zinc sulfate	0.5 mol/l	Temperature	40 ºC
Nickel sulfate	0.5 mol/l	Anode Zn	
pH 4.5		pure Ni, S-containing Ni	
Chloride bath:			
Zinc chloride	0.5 mol/l	Cathode Cu	
Nickel chloride	0.5 mol/l		
pH 4.5		Quiescent bath	

than 100 %. This leads to a gradual decrease in the concentration of one of the constituents and increase in that of the other when one of the constituents is used as a soluble anode, and the second constituent is replenished by additions of chemicals. Hence in this study, a coupled anode system composed of both constituents was adopted in Zn-Ni alloy plating and the anodic dissolution efficiency was examined. Bath composition and operating conditions are shown in Table 8. In the coupled anode system composed of Zn and Ni, each anode was equipped with a variable resistance to control independently the anodic current density applied. Pure Zn, pure Ni and 0.02 % S-containing Ni produced by Sumitomo Metal Mining Co., Ltd.

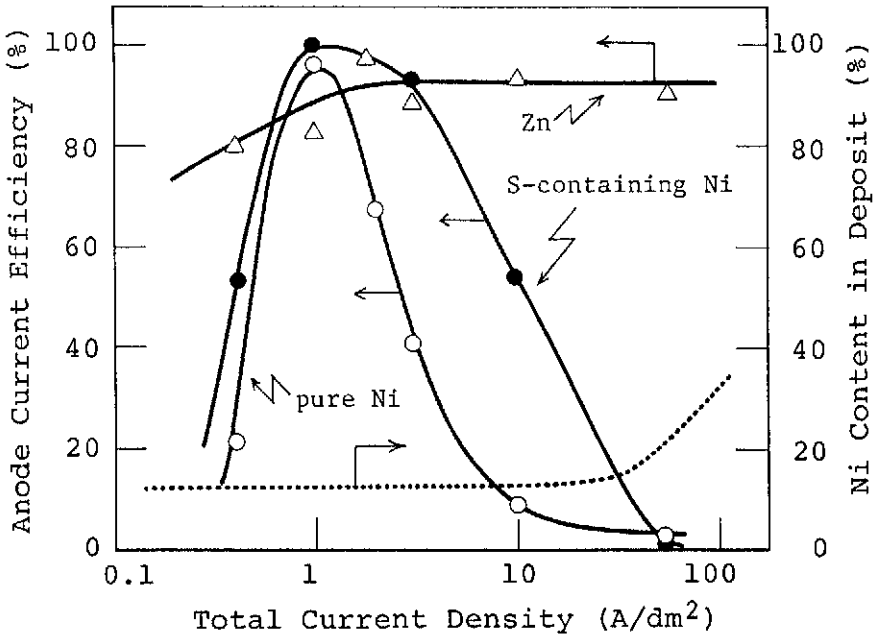

Fig.35 Effect of current density on the anode current efficiency of Zn, pure Ni and S-containing Ni in sulfate baths.

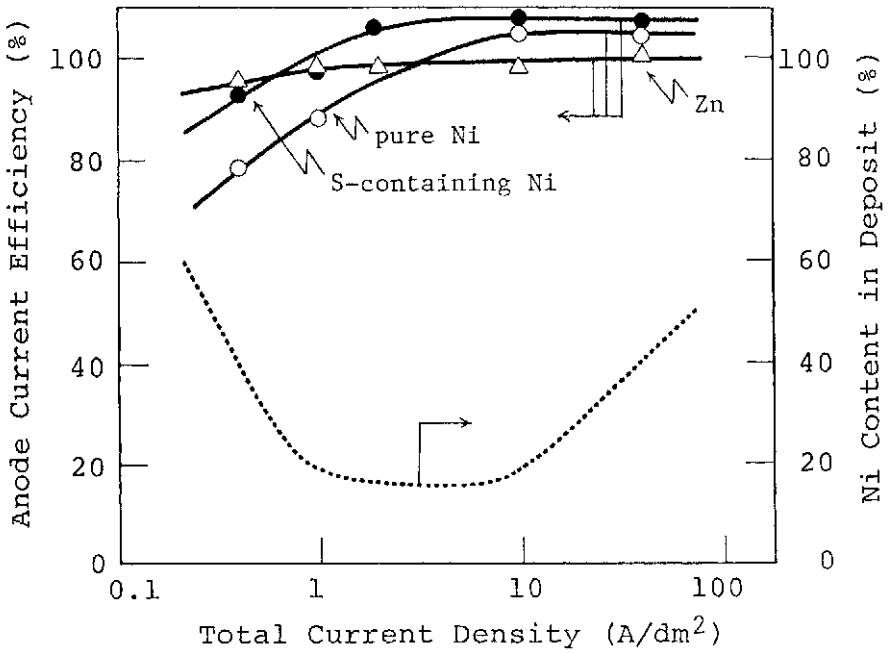

Fig.36 Effect of current density on the anode current efficiency of Zn, pure Ni and S-containing Ni in chloride baths.

(Trademark: SK nickel) were used as anode materials and dissolution efficiencies were determined by measuring the weight loss of each anode.

Figures 35 and 36 show the anode dissolution efficiencies at various cathode current densities in sulfate and chloride baths, respectively. Alloy composition change is also presented by a dotted line in these figures. In this experiment, total anode current density is distributed to each anode in accordance with the corresponding alloy composition so as to minimize the change in each metal ion concentration in the bath. When the alloy contains 10 % Ni, for example, the partial cathodic current density ratio of Ni to Zn is 1:9. Then, 10 % of the total anodic current was applied to Ni and 90% to Zn. Further, anodic current efficiency of each anode in these figures was calculated under the assumption that it became 100 % when all current applied to each anode was consumed by metal dissolution.

In the sulfate bath, as shown in Fig.35, dissolution efficiency of Zn was ca. 80 % in the low current density region below 1 A/dm^2 and increased gradually with increasing current density. Pure and S-containing Ni anodes showed maximum dissolution efficiency of ca. 100% at 1 A/dm^2 . Either decreasing or increasing current density from this optimum value resulted in an abrupt decrease in dissolution efficiency. Decrease in the dissolution efficiency at higher current densities must be caused by passivation of the anode although the reason for the decrease at lower current densities is obscure at the moment.

In chloride baths, as shown in Fig.36, Zn dissolved with ca. 100% efficiency over the current density range examined. The dissolution efficiency of pure and S-containing Ni anodes increased with

increasing current density and exceeded 100 % at current densities above 2 A/dm^2. In chloride baths, no decrease in the dissolution efficiency of Ni was observed at high current densities because Cl ion prevented the passivation of Ni. Dissolution efficiency was a little higher for S-containing Ni than for pure Ni, which was the same trend as observed in sulfate baths.

3-4-2 Deposition of Ni on soluble Zn anodes.

In the electrodeposition of Zn-Ni alloys using soluble Zn anodes, the cathodic alloy deposition in region II proceeds at potentials somewhat less noble than the equilibrium value of Zn while anodic Zn dissolution proceeds at potentials somewhat more noble than the equilibrium value of Zn. Considering that Zn has a quite negative equilibrium potential, Ni can be deposited on the anode Zn as well as on the cathode.

Therefore, the Zn anode was dissolved with hydrochloric acid after finishing galvanostatic (1 and 10 A/dm^2) and coulostatic (100 C/cm^2) electrolysis using the coupled anode system, and Ni in the resultant solution was analyzed to confirm Ni deposition. Results are shown in Table 9 for two different Ni anode materials, the pure Ni and S-containing Ni. The table also contains the apparent and corrected Zn dissolution efficiency.

The amount of deposited Ni on the Zn anode is almost independent of the Ni anode materials, indicating that displacement deposition of Ni onto the Zn is not influenced by the type of Ni anode.

Table 9 Amount of deposited Ni on the Zn anode and the correction of apparent anode current efficiency for Zn deposition.

Sulfate bath:

Current density (A/dm^2)	Amount of deposited Ni on Zn anode (mg/cm^2)	Apparent anode current eff. of Zn (%)	Corrected anode current eff. of Zn (%)
1	0.616* 0.578**	83.6* 82.0**	85.4* 83.7**
10	0.316* 0.399**	96.6* 90.0**	97.7* 91.2**

Chloride bath:

Current density (A/dm^2)	Amount of deposited Ni on Zn anode (mg/cm^2)	Apparent anode current eff. of Zn (%)	Corrected anode current eff. of Zn (%)
1	1.16* 1.39**	98.2* 98.7**	101.6* 102.7**
10	1.43* 1.35**	98.8* 96.7**	103.0* 100.3**

* Pure Ni, ** S-containing Ni

As shown in Table 9, Ni deposition of 0.3 - 0.6 mg/cm^2 in the sulfate bath and of 1.2 - 1.4 mg/cm^2 in the chloride bath was observed on the Zn anode. Therefore, actual Zn dissolution efficiency is 1 – 2% higher in the sulfate bath and 3 - 4 % higher in the chloride bath than the apparent values. A larger amount of Ni was thus deposited on the Zn anode during alloy deposition in the chloride bath than in the sulfate bath. Considering that Ni deposition proceeds around the equilibrium potential of Zn on both cathode and anode in the presence of large amounts of Zn ions, Ni deposition behavior on a Zn anode should be explained from analogy with its cathodic deposition. During alloy deposition in region I, as mentioned in 3-3-2, larger amount of Ni is deposited on the cathode from a chloride bath than from a sulfate bath, which is in good agreement with the deposition behavior of Ni on a Zn anode. Thus, the properties peculiar to the iron-group metal are also reflected in the reaction at a Zn anode.

From the standpoint of dissolution efficiency, as mentioned previously in this section, the chloride bath is preferable to the sulfate bath when a soluble Zn anode is adopted, in order to minimize the bath composition change. However, Ni deposition occurs on Zn anodes, which may fall away from the anode to bring about scratches on the plated surface when it comes between the sheet to be plated and a conductor or guiding roll during continuous plating operations. In batch plating, an anode bag which prevents the suspension of Ni particles seems to be necessary in the sulfate and especially in the chloride bath.

4. Structure and corrosion behavior of electrodeposited Zn-Ni alloys.

The structure of Zn-Ni alloy films electrodeposited from sulfate baths has been studied. The alloy films were deposited in the bath at pH 3.0 or 4.5, either at a constant cathodic current density, or continuously changing current densities. To obtain a range of continuously changing current densities, a Hull cell was used. The structure was examined by X-ray diffraction, and surface morphology and composition were examined using SEM and EPMA.

To understand the fundamental properties of the corrosion of the electrodeposited films, corrosion behavior of the films without any topcoat was studied in aqueous solutions.

4-1. Structure of electrodeposited films.

For the specimens prepared using a Hull cell distribution of the current density, contents of Ni and Zn, alloy composition and thickness of the deposited film as a function of the distance from the edge of high current density side of the specimen are shown in Fig.37. Thickness of the deposited film changes with current density, but the concentration of Ni does not change much with the change in current density. Surface appearance of the film deposited in the pH 3.0 bath is shown in Photo.2. In the high current density region the deposit shows fine irregular appearance. In the region of current density 15~5A/dm^2 the deposit appears granular, and the grain size decreases as the current density decreases.

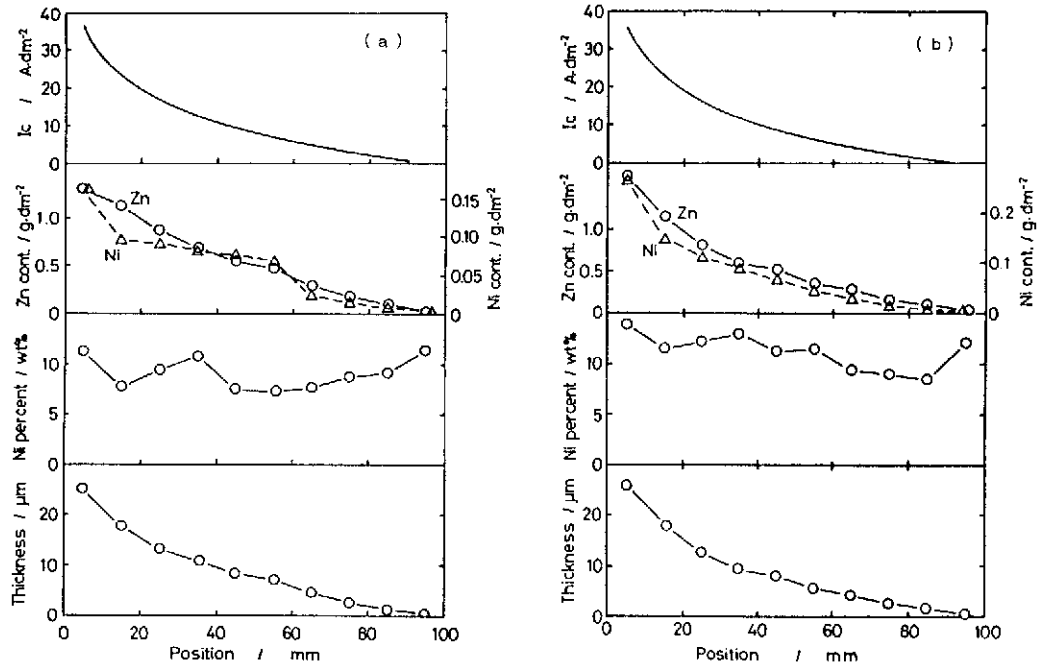

Fig.37 Distribution of current density, contents of Zn and Ni, alloy composition and thickness of the deposited film as a function of the distance from the edge of high current density side of the specimen. (a) bath at pH 3.0, (b) bath at pH 4.5.

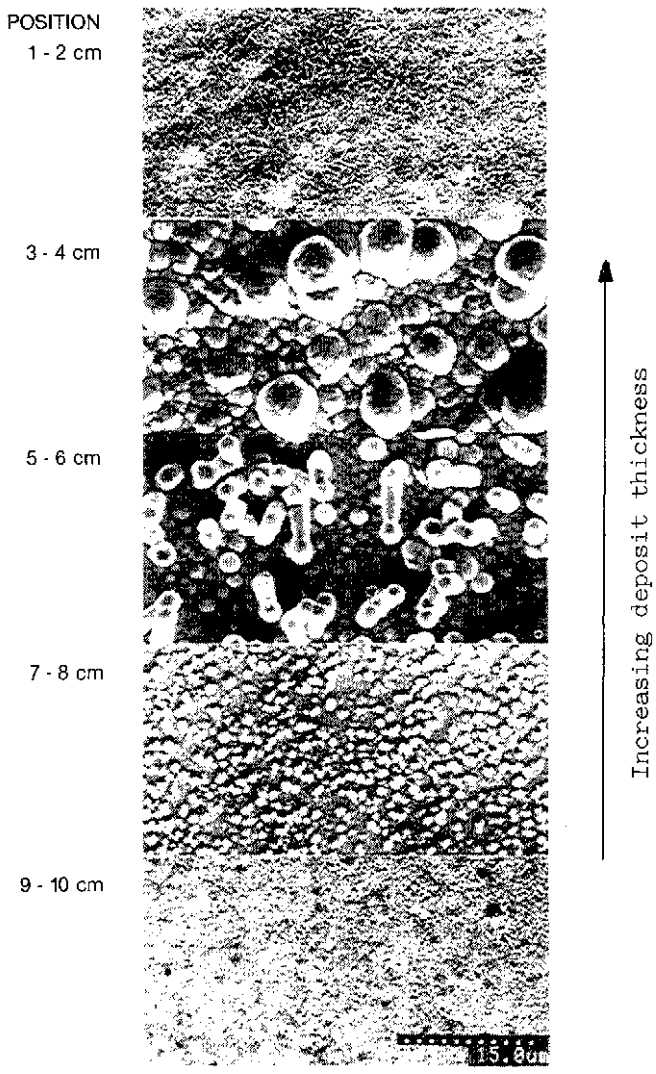

Photo.2 Surface appearance of the film deposited in a Hull cell; change of the position corresponds to the difference in current density.

Distribution of Ni and Zn over the surface was examined by EPMA, and the result is shown in Photo.3 for the film deposited with current density around 10 A/dm^2. Two-dimensional distribution of Ni and Zn was homogeneous. Depth distribution of alloying elements was also examined on the cross-sectional face. The result showed some scattering, but in most cases Ni content was high near the interface with the substrate.

Alloy phases were examined by X-ray diffraction. Figure 38 shows the X-ray diffraction profiles of the deposits taken from various positions on the films plated in a Hull cell with the baths at pH 3.0 and 4.5. The deposited film consists of Zn, $Ni_3Zn_{22}(\delta)$ and $Ni_5Zn_{21}(\gamma)$ as reported by other workers [41]. Additionally, $Zn(OH)_2$ and unidentified phase are observed. The relation between the formation of intermetallic compounds and current density is not clear, but high Ni concentration is related to the formation of gamma phase.

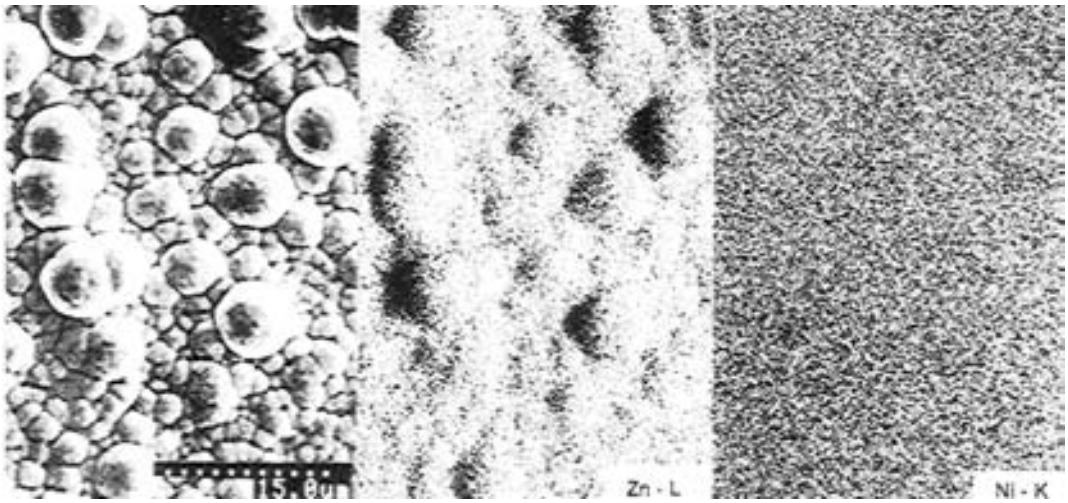

Photo.3 Distribution of Zn and Ni over the surface of electrodeposited film. An SEM image and Zn-L, Ni-K X-ray maps are shown.

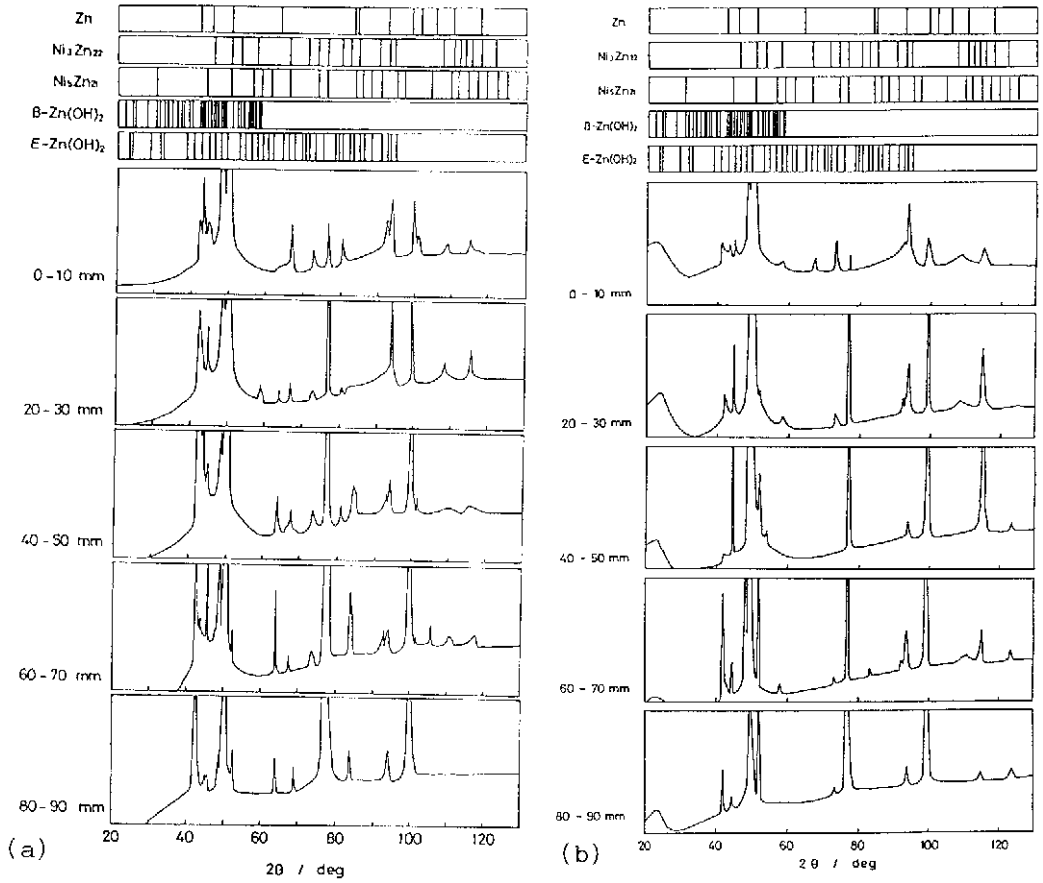

Fig.38 X-ray diffraction profiles of the deposits from various position of the deposited film. (a) deposited in the bath at pH 3.0, (b) deposited in the bath at pH 4.5.

4-2. Corrosion properties of Zn-Ni electrodeposited films.

To understand the fundamental corrosion properties of Zn-Ni alloy coatings, the corrosion process of the films in pH 6 aqueous buffer solution and 3% NaCl solution was studied. Specimens were prepared by electroplating either at constant current density or at continuously changing current densities in a Hull cell. The Hull cell specimens were used either by cutting into pieces at various positions corresponding to different current densities or without cutting as inhomogeneous specimens.

Change of corrosion potentials of plated films, comprising Zn-Ni plated onto Cu and Fe substrates and Zn plated on Fe, as a function of immersion time in the pH 6 buffer solution and 3% NaCl solution is shown in Fig.39. The corrosion potential of simple Zn film retains base potential as long as Zn remains on the surface. On alloy films however, the potential shifts to more noble values soon after immersion, and eventually attains a constant potential. When the substrate is Cu the corrosion potential shifts further to noble values and reaches the corrosion potential of Cu. In the case of Fe

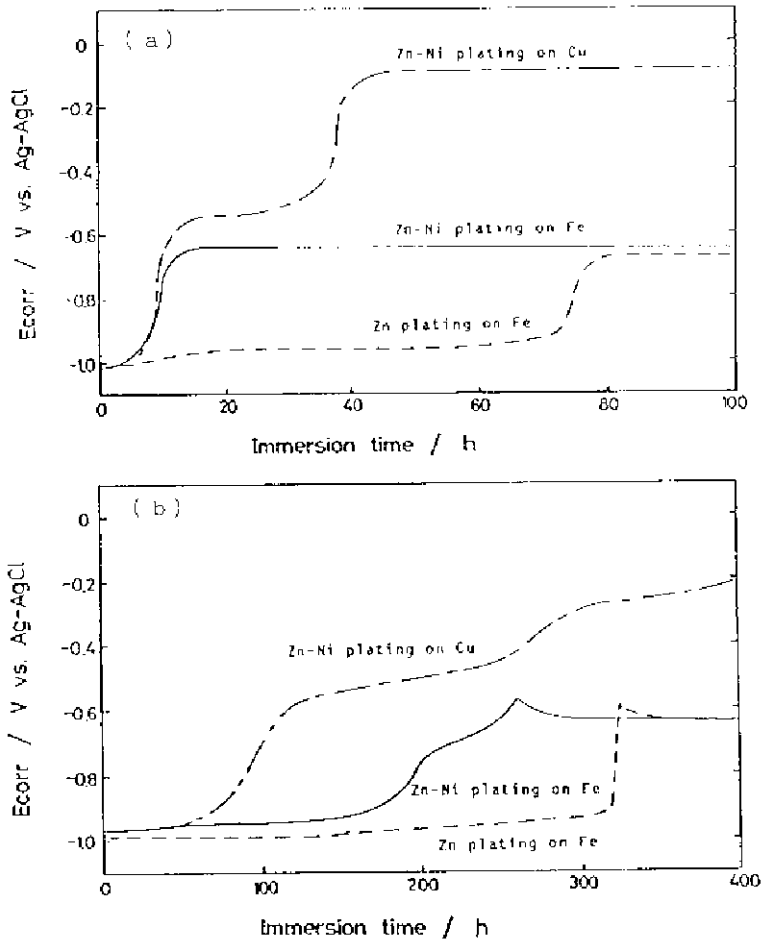

Fig.39 Change of corrosion potential of coated films as a function of immersion time in pH 6 buffer solution (a), and in 3% NaCl solution (b). Ni-Zn alloy was plated onto Cu and Fe substrates and Zn was plated onto Fe.

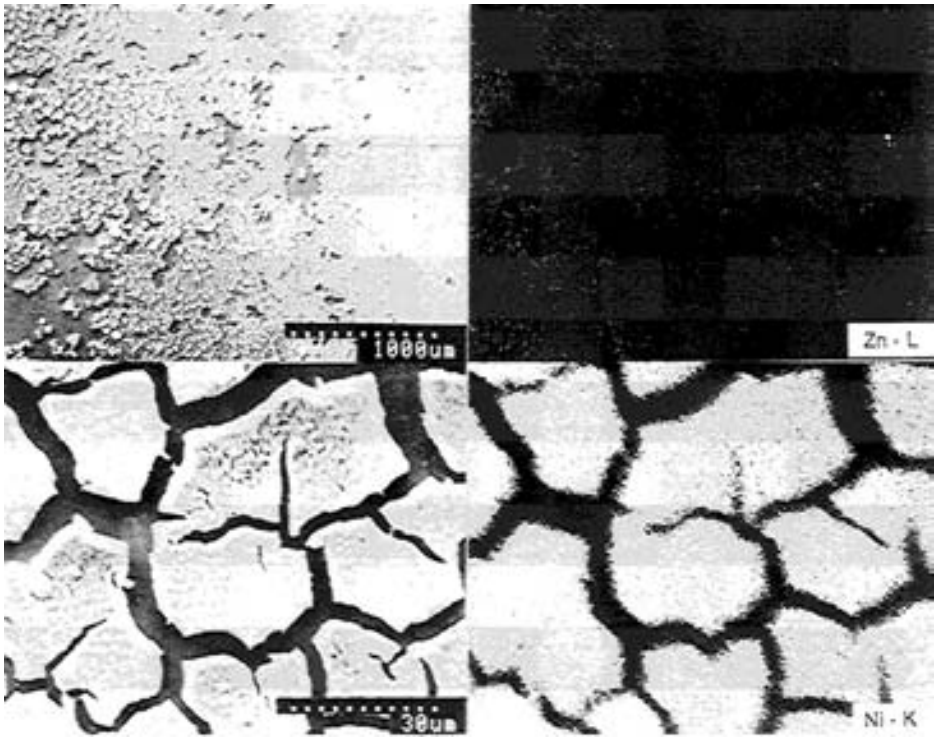

Photo.4 SEM image and Zn-L, Ni-K X-ray maps of the specimen corroded in the buffer solution.

substrates, the stationary potential of the film is close to the corrosion potential of the substrate Fe, so that the potential duration is not clear. That is, in alloy films, corrosion potential moves in the more noble direction even if Zn remains on the surface, and attains a stationary value, which is attributed to the corrosion potential of the corroded film. This can be clearly seen in Photo.4, which shows SEM images of low and high magnification and Zn-L, Ni-K characteristic X-ray maps corresponding to an enlarged SEM image of the specimen which had been immersed in the buffer solution until the corrosion potential attained a stationary value. As corrosion proceeds on such a specimen, corrosion potential shifts to more noble values, that is, anodic reaction of Zn dissolution is polarized by the formation of corrosion products and cathodic reaction is depolarized by the presence of Ni. The corrosion takes place inhomogeneously making corrosion grooves. The films remaining as islands are enriched in nickel content. Thus Zn-Ni alloy coating can be said to be changed to a noble surface by corrosion.

Corrosion potential was measured for alloy films taken from various positions on a Hull cell specimen, and the results are shown in Fig.40. All the specimens showed a similar variation of the corrosion potential. The difference in time may be due to the difference of the amount of Zn in the films. Surface appearance of these specimens in the course of corrosion is shown in Photo.5. Corrosion took place inhomogeneously making corrosion grooves in all specimens. The corrosion grooves are coasely distributed in thicker film, more finely distributed as the coating film become thinner.

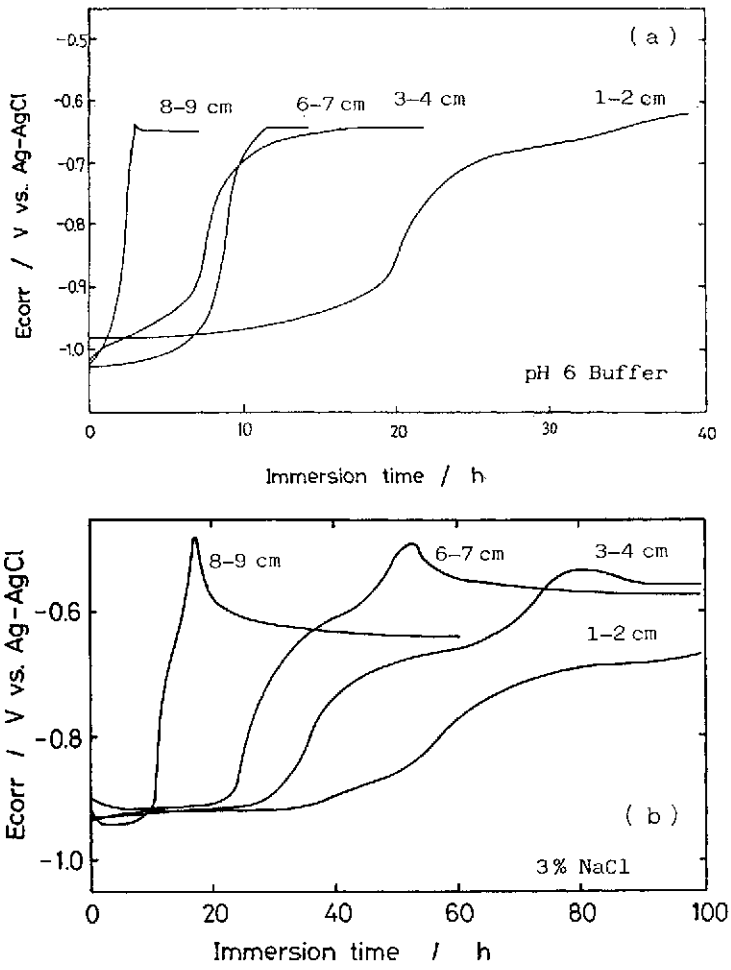

Fig.40 Change of corrosion potential during immersion in pH 6 buffer solution (a) and in 3% NaCl solution (b) for plated films taken from various positions on the Hull cell specimen.

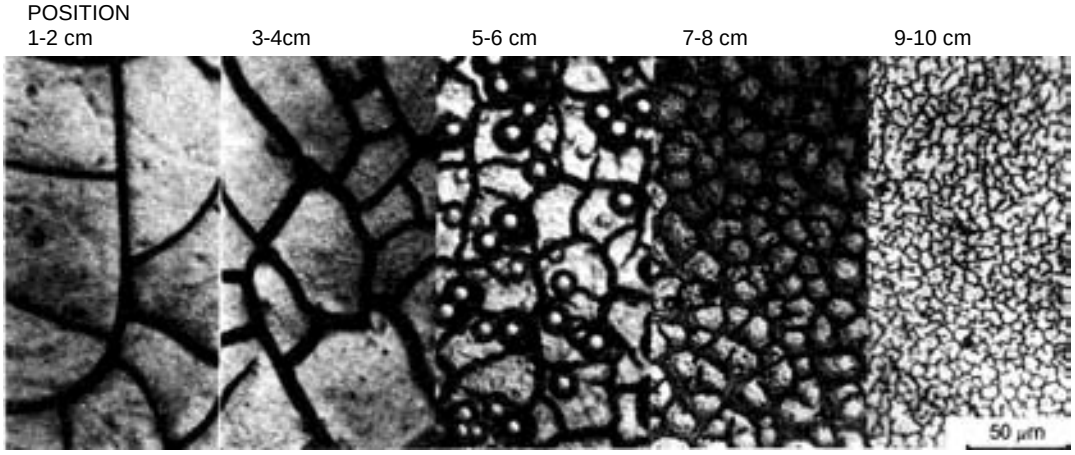

Photo.5 Surface appearance of the corroded coatings which were taken from various positions on a Hull cell specimen and separately immersed in the corrosive solution.

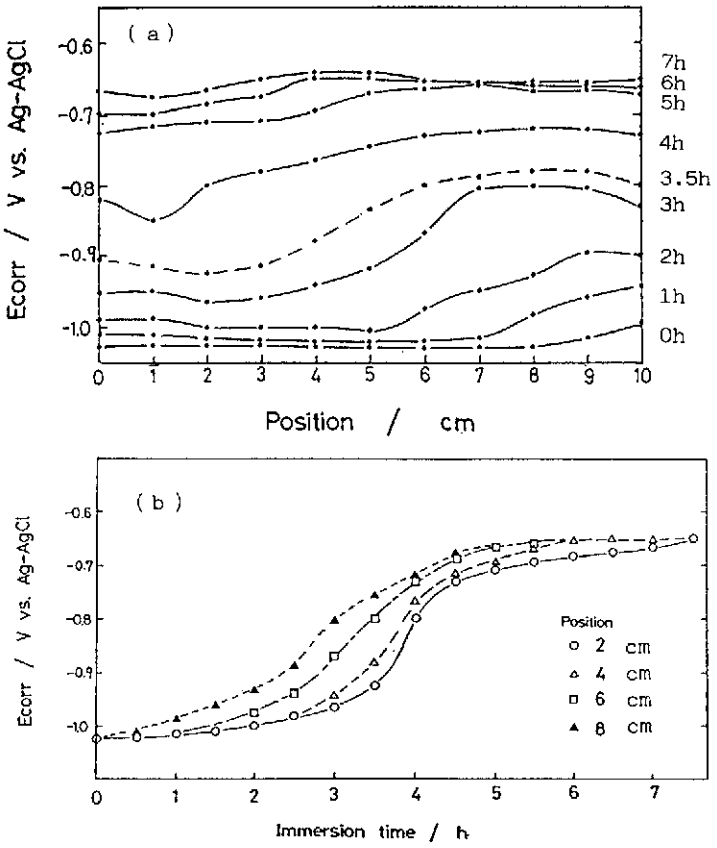

Fig. 41 (a) Distribution of corrosion potential along the specimen electroplated in a Hull cell after certain interval of immersion time. (b) Change of corrosion potential at various positions on the specimen as a function of immersion time.

To study the effect of inhomogenity of the coating on corrosion properties, immersion tests were carried out on specimens electroplated in a Hull cell with continuously varying current densities. Corrosion potentials at various positions on the specimen, along the direction of varying current density, were measured after certain intervals of time of immersion. Figure 41 shows distribution of corrosion potential along the direction of varying film thickness (a), and the change of the potentials at various positions against immersion time (b). Corrosion potential moves to more noble values first at the region of thin coating, and a macro-cell of corrosion is formed along the specimen length. By the formation of the macro-cell, corrosion proceeds faster than in the case of homogeneous coatings. Corrosion form in this case is also by development of corrosion grooves. Since a microscopical corrosion cell is formed along the grooves and the macro-cell action is superposed upon it, the corrosion process in an inhomogeneous coating is complicated. An example of this complication is that red rust appears in a thick coating region when the inhomogeneous specimens are immersed in 3% NaCl solution. This is schematically illustrated in Fig.42; appearance and extension of the red rust region during the progress of corrosion is indicated. The red rust starts to appear in a thick coated region where the film remains in the region as islands separated by grooves.

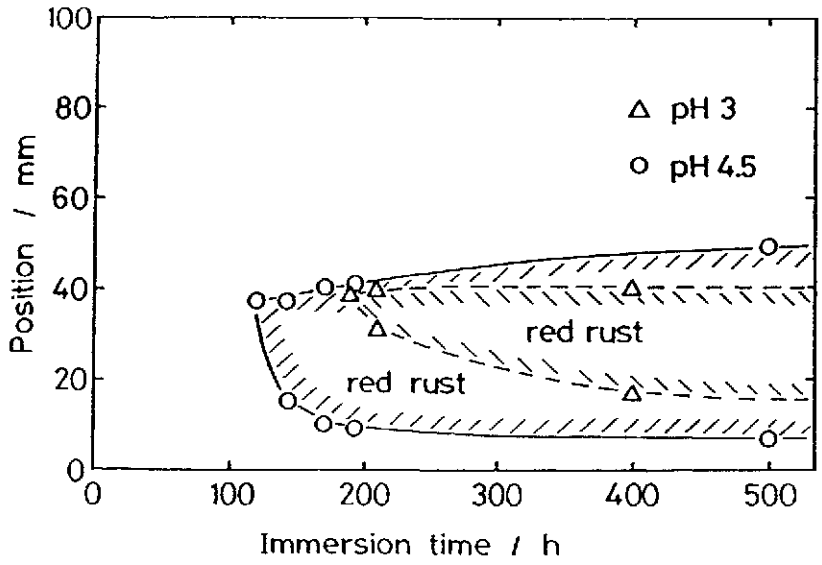

Fig.42 Change in the red rust zone on the specimens electroplated in a Hull cell with baths of pH 3.0 and 4.5, during corrosion in a 3% NaCl solution.

The corrosion properties of Zn-Ni coatings can be summarized as follows: (1) By alloying, the initial corrosion is accelerated and the coating easily changed to an electrochemically more noble surface; (2) Corrosion proceeds inhomogeneously and forms a crack-like corrosion groove. These two characteristics play a complicated role in the improvement of corrosion resistance in most corrosion environments.

4-3. Comparison with other Zn alloy platings.

Corrosion properties of Zn alloy electroplated films have been studied [38, 42-45] for a variety of alloy systems for various purposes. Comparison of the properties of electrodeposited Zn-Co, Zn-Fe and Zn-Ni alloys is interesting. Table 2 and Photo.6 show the compositions of plating baths and surface appearances of the electrodeposits. Corrosion tests were carried out in pH 6 buffer solution. Figure 43 shows change of corrosion potentials of Zn and Zn alloys electrodeposited on Fe (a) and Cu (b) substrates. The alloy deposits show a similar variation of potential, but its rate differs with the alloying element. The surface appearance of the coatings after corrosion is shown in Photo.7. The form of corrosion is the same

Table 10 Electroplating conditions.

(a) Bath composition

	Zn	Zn-Co	Zn-Ni	Zn-Fe
$ZnSO_4 \cdot 7H_2O$	1 kmol/m^3	0.5 kmol/m^3	0.5 kmol/m^3	0.79 kmol/m^3
$CoSO_4 \cdot 7H_2O$		0.5 kmo1/m^3		-
$NiSO_4 \cdot 7H_2O$			0.5kmol/m^3	-
$FeSO_4 \cdot 7H_2O$				1.01 kmol/m^3
Na_2SO_4				0.21 kmol/m^3
$CH_3COONa\text{-}3H_2O$	0.2 kmol/m^3	0.2 kmol/m^3	0.2 kmol/m^3	0.09 kmol/m^3

(b) Operating conditions : Current density 1 kA/m^2, temperature 313 K, pH 3.0

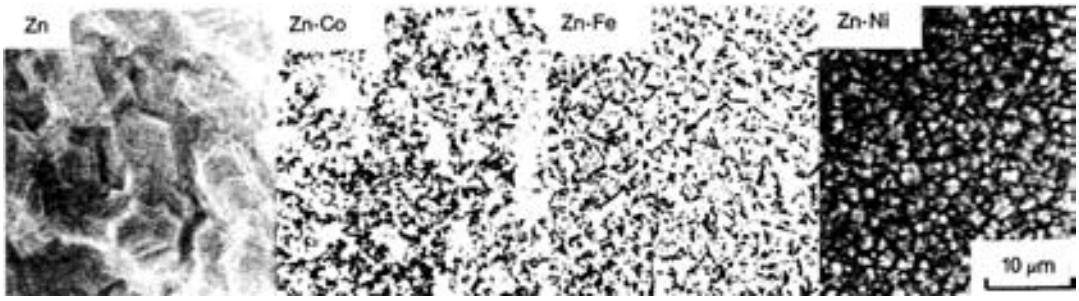

Photo.6 Surface appearance of the electrodeposits of Zn, Zn-Co, Zn-Fe and Zn-Ni.

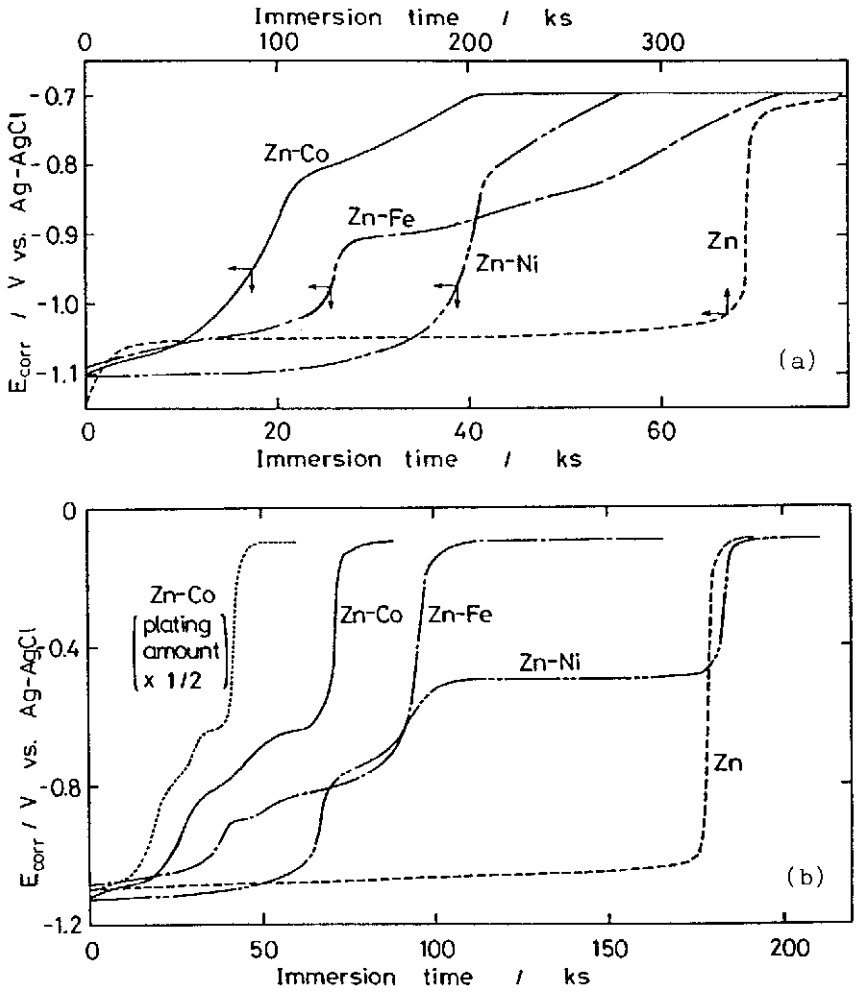

Fig.43 Change of corrosion potentials of Zn and Zn alloys electrodeposited on Fe (a) and Cu (b) substrates.

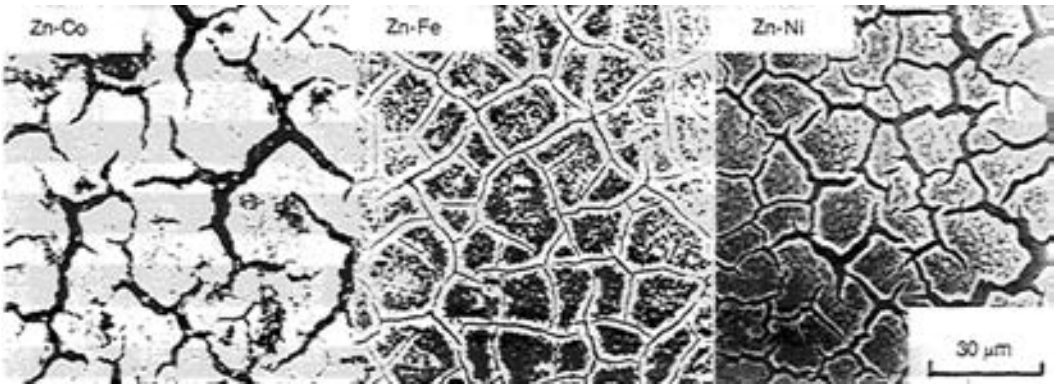

Photo.7 Surface appearance of the coatings of Zn-Co, Zn-Fe and Zn-Ni after corrosion.

for Zn-Co, Zn-Fe and Zn-Ni alloys; corrosion proceeds inhomogeneously making corrosion grooves. Duration of the coating film of Zn-Ni alloy in the course of corrosion is the longest among the alloys, and the best performance can therefore be expected from Zn-Ni coating.

Acknowledgment

The authors wish to express their thanks to Dr. S. Alec. Watson, Proprietor of the Watson Consultancy Service, West Midlands, England for helpful discussion.

Reference

1) A. Krohn and C. W. Bohn: Electrodepo. Sur. Treat., Vol.**l**, 119 (1972/73)
2) M. Nishikawa and A. Matsuno: Bull. Japan Inst. Metals, Vol.**21**, 512 (1982)
3) K. Horikawa: J. Metal Finishing Soc., Vo1.**33**, 360 (1982)
4) W. R. Johnson and J. B. Vrable: SAE Tech. Pap. Ser., No. 840213 (1984)
5) M. Toda, H. Kojima, T. Morishita, T. Kanamura and K. Arai: ibid., No.840212 (1984)
6) R. Noumi, H. Nagasaki, Y. Foboh and A. Shibuya: ibid., No. 820332 (1982)
7) A. Brenner: "Electrodeposition of Alloys", Vol. **l** & **2**, (1963), Academic Press
8) M. Pourbaix: "Atlas of Electrochemical Equilibria", (1966), Pergamon Press
9) J. M. West: "Electrodeposition and Corrosion Processes" 2nd Ed., (1977), p.122, Sangyou Tosho Pub. Co.
10) T. Oki: "Electrochemistry of Metal", (1971), p.82, Kyouritsu Pub. Co.
11) H. B. Mark Jr. and C. N. Reilley: Anal. Chem., Vol.**35**, 195 (1963)
12) H. B. Mark Jr.: Electroanal. Chem., Vol.**7**, 276 (1964)
13) L. R. McCoy and H. B. Mark Jr.: J. Phys. Chem., Vol.**72**, 4637 (1968)
14) D. C. Olson: Anal. Chem., Vol.**39**, 1785 (1967)
15) Ya. I. Tur'yan and O. N. Malyavinskaya: Electrochimica Acta, Vol.**17**, 1181 (1972)
16) R. Revie: J. Electrochem. Soc., Vol.**118**, 185C (1971)
17) M. von Stackelberg, W. Hans and W. Jensch: Zeit. Elektrochem., Vol.**62**, 839 (1958)
18) C. Kittel: "Introduction to Solid State Physics", 2nd ed., (1956), p.335, John Wiley & Sons Inc.
19) P. Ruetschi and P. Delahay: J. Chem. Phys., Vol.**23**, 195 (1955)
20) H.Suetaka: Bull. Japan Inst. Metals, Vol.**12**, 801 (1973)
21) K. Higashi and H. Fukushima: J. Metal Finishing Soc., Japan, Vo1.**24**, 486 (1973)
22) K. Higashi, H. Fukushima, H. Ohashi and T. Akiyama: ibid., Vol.**27**, 590 (1976)
23) K. Higashi, H. Fukushima and K. Kitamura: ibid., Vo1.**28**, 112 (1977)
24) H. Fukushima, T. Akiyama, S. Akagi and K. Higashi: Trans. Japan Inst. Metals, Vo1.**20**, 358 (1979)
25) H. Fukushima, T. Akiyama, H. Nakakoji and K. Higashi: J. Metal Finishing Soc. Japan, Vol.**30**, 600 (1979)
26) H. Fukushima, T. Akiyama and K. Higashi: ibid., Vol.**32**, 58 (1981)
27) T. Akiyama, H. Fukushima and K. Higashi: J. Iron Steel Inst. Japan, Vol.**72**, No.8, 918 (1986)

28) L. Li, T. Akiyama, H. Fukushima and K. Higashi: J. Metal Finishing Soc. Japan, Vol.**37**, 660 (1986)
29) H. Dahms and I. M. Croll: J. Electrochem. Soc., Vol.**112**, 771 (1965)
30) D. E. Hall: Plat. Surf. Finishing, Vol.**70**[11], 59 (1983)
31) K. Higashi, H. Fukushima, T. Urakawa, T. Adaniya and K. Matsydo: J. Electrochem. Soc., Vol.**128**, 2081 (1981)
32) H. Fukushima, T. Akiyama, J. Lee, M. Yamaguchi and K. Higashi: Trans. Japan Inst. Metals, Vol.**24**, 125 (1983)
33) K. Higashi, H. Fukushima, T. Akiyama and E. Hino: J. Corrosion Protection Western Japan, No.7, 1 (1977)
34) H. Fukushima, T. Akiyama, K. Higashi, M. Karimkhani and R. Kammel: Metall, Vol.**42**, 242 (1988)
35) T. Akiyama, H. Fukushima, J. Lee and K. Higashi: J. Metal Finishing Soc. Japan, Vol.**37**, 20 (1986)
36) L. Li, T. Akiyama, H. Fukushima and K. Higashi: ibid., Vol.**37**, 660 (1986)
37) S. K. Panikkar and T. L. Rama Char: ibid, Vol.**25**, 573 (1957)
38) A. Shibuya, T. Kurimoto, K. Korekawa and K. Noji: J. Iron Steel Inst. Japan, Vol.**66**, 771 (1980)
39) A. Shibuya and T. Kurimoto: J. Metal Finishing Soc. Japan, Vol.**33**, 544 (1982)
40) A. F. Bogenschutz and U. George: "Galvanische Legierungsabscheidung und Analytik", 2nd ed., (1982), p.153, Eugen G. Leuze Verlag
41) T. Hara, M. Sagiyama and T. Adaniya: Bull. Japan Inst. Metals, Vol.**27**, 258 (1988)
42) Y. Miyoshi, J. Oka and S. Maeda: Trans. Iron Steel Inst. Janan, Vol.**23**, 974 (1983)
43) T. Adaniya, M. Sagiyama and T. Homma: Nippon Kokan Giho, Vol.**105**, 797 (1984)
44) K. Ariga and K. Kanda: J. Iron Steel Inst. Japan, Vol.**66**, 797 (1980)
45) H. Hagi, K. Inokuchi, Y. Hayashi and K. Higashi: ibid, Vol.**73**, 118 (1987)